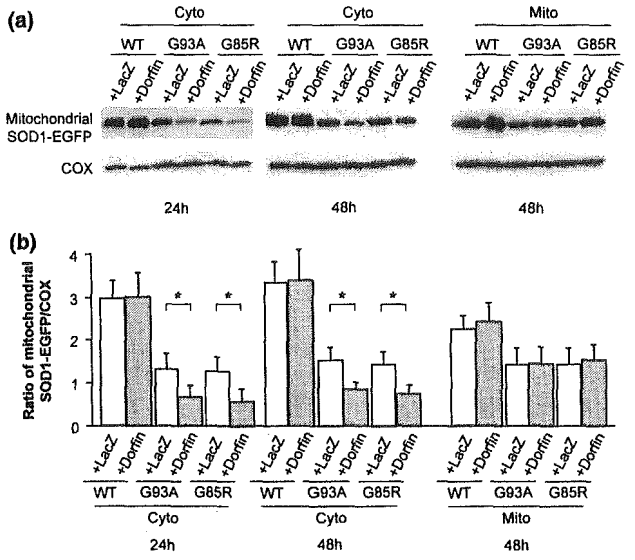

Fig. 4 Level of mitochondrial SOD1-EGFP fusion protein. (a) Levels of mitochondrial SOD1-EGFP fusion protein. (b) Densitometric analysis of mitochondrial SOD1-EGFP fusion protein expressed as a ratio to COX. In the mitochondrial fraction, Dorfin significantly reduced the level of SOD1-EGFP fusion protein expressed by Cyto-G93A or Cyto-G85R, whereas it did not reduce that expressed by Mito-SOD1. Values are mean ± SD ($n = 4$). *$p < 0.05$ (two-way ANOVA with Tukey–Kramer post-hoc test).

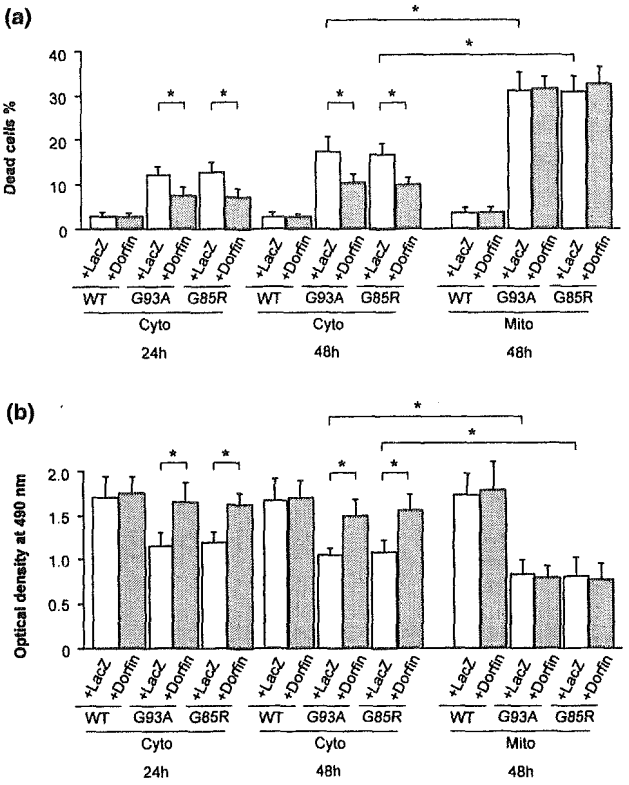

Fig. 5 (a) Frequency of dead cells and (b) mitochondrial impairment analyzed by MTS assay. The cells with Mito-G93A and Mito-G85R exhibited a significantly higher level of cell death and mitochondrial impairment than those with Cyto-G93A and Cyto-G85R. Dorfin significantly decreased cell death and mitochondrial impairment induced by Cyto-G93A and Cyto-G85R, whereas it did not affect those induced by Mito-SOD1. Values are mean ± SD ($n = 6$). *$p < 0.05$ (two-way ANOVA with Tukey–Kramer post-hoc test).

Dorfin protects neuronal cells from mutant SOD1-mediated neurotoxicity by reducing mitochondrial mutant SOD1

As we demonstrated previously (Takeuchi *et al.* 2002a), the cells with Cyto-G93A and Cyto-G85R underwent cell death (Fig. 5a) and mitochondrial impairment (Fig. 5b), whereas those with Cyto-WT did not. The cells with Mito-G93A and Mito-G85R exhibited significantly more cell death and mitochondrial impairment than those with Cyto-G93A and Cyto-G85R, whereas those with Mito-WT did not (Fig. 5). Co-expression of Dorfin significantly ameliorated cell death and mitochondrial impairment induced by Cyto-G93A and Cyto-G85R (Fig. 5), as in our previous report (Niwa *et al.* 2002). In contrast, Dorfin did not affect cell death and mitochondrial impairment induced by Mito-SOD1 (Fig. 5), whose protein level Dorfin did not reduce. These findings suggest that Dorfin ameliorates mutant SOD1-mediated neurotoxicity by reducing the accumulation of mutant SOD1 in the mitochondria.

Dorfin reduces mitochondrial cytochrome *c* release and sequential activation of caspase-9 and caspase-3

We next assessed whether Dorfin reduced the mitochondrial death signal associated with the mutant SOD1-mediated cytotoxicity. Western blots revealed that Cyto-G93A and Cyto-G85R induced a gradual increase in the cytochrome *c* released from the mitochondria into the cytosol, whereas Cyto-WT did not (Fig. 6). The cells with Mito-G93A and Mito-G85R also exhibited a higher level of cytochrome *c* release than those with Cyto-G93A and Cyto-G85R, whereas those with Mito-WT did not (Fig. 6). Co-expression of Dorfin significantly reduced the release of cytochrome *c* from the mitochondria into the cytosol induced by Cyto-G93A and Cyto-G85R (Fig. 6). In the cells with Mito-G93A and Mito-G85R, however, Dorfin did not reduce the cytochrome *c* release from the mitochondria into the cytosol (Fig. 6).

Next, we examined whether Dorfin affected the downstream signal cascade of the activation of caspase-9 and caspase-3 following the release of mitochondrial cytochrome *c*. As we demonstrated previously (Takeuchi *et al.* 2002a), western blots revealed that Cyto-G93A and Cyto-G85R induced gradual activation of caspase-9 and caspase-3, whereas Cyto-WT did not (Figs 7 and 8). The cells with Mito-G93A and Mito-G85R exhibited a higher level of activation of caspase-9 and caspase-3 than those with Cyto-G93A and Cyto-G85R, whereas those with Mito-WT did not (Figs 7 and 8). Co-expression of Dorfin significantly reduced

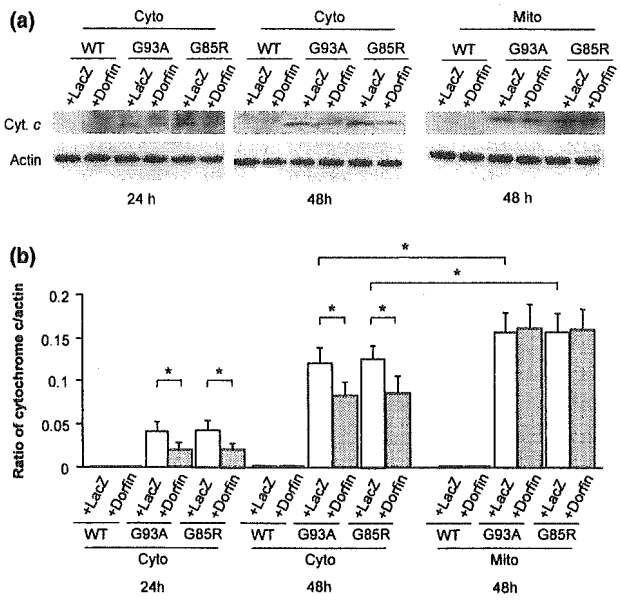

Fig. 6 Western blot analysis of cytochrome *c* release. (a) Time course of mitochondrial cytochrome *c* release into the cytosol. (b) Densitometric analysis of cytochrome *c* release expressed as a ratio to COX. The cells with Mito-G93A and Mito-G85R exhibited significantly more cytochrome *c* release than those with Cyto-G93A and Cyto-G85R. Dorfin significantly reduced the amount of mitochondrial cytochrome *c* released into the cytosol induced by Cyto-G93A and Cyto-G85R, whereas it did not affect that induced by Mito-SOD1. Values are mean ± SD ($n = 4$). $^*p < 0.05$ (two-way ANOVA with Tukey–Kramer post-hoc test).

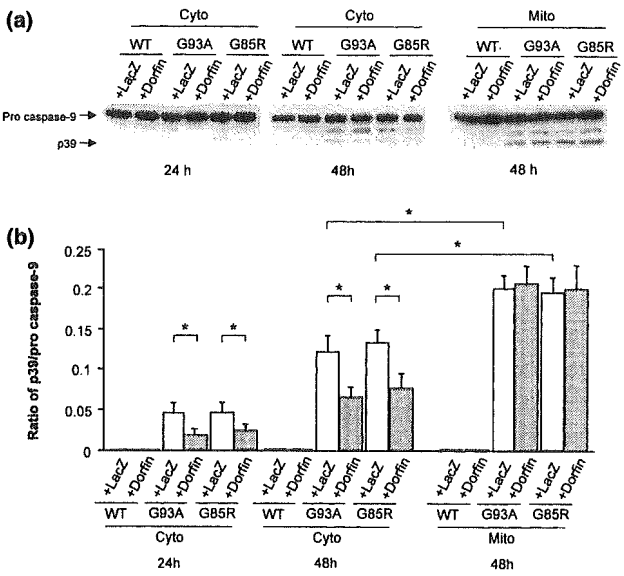

Fig. 7 Western blot analysis of caspase-9 activation. (a) Time course of the activation of caspase-9. (b) Densitometric analysis of caspase-9 activation. The cells with Mito-G93A and Mito-G85R exhibited significantly more activation of caspase-9 than those with Cyto-G93A and Cyto-G85R. Dorfin significantly reduced the activation of caspase-9 induced by Cyto-G93A and Cyto-G85R, whereas it did not reduce that induced by Mito-SOD1. Values are mean ± SD ($n = 4$). $^*p < 0.05$ (two-way ANOVA with Tukey–Kramer post-hoc test).

the activation of caspase-9 and caspase-3 induced by Cyto-G93A and Cyto-G85R (Figs 7 and 8). However, Dorfin did not reduce the activation of caspase-9 and caspase-3 induced by Mito-G93A and Mito-G85R (Figs 7 and 8), as it did not reduce the release of cytochrome *c* induced by Mito-G93A and Mito-G85R (Fig. 6). These findings combined with the aforementioned observations suggest that the reduction in the amount of mitochondrial mutant SOD1 due to Dorfin results in attenuated activation of the mitochondrial PCD pathway and prevents eventual cell death.

Discussion

In the present study, we first demonstrated that Dorfin, an E3 for mutant SOD1s, attenuated the activation of the mitochondrial PCD pathway and prevented eventual cell death in a neuronal cell model of FALS by reducing the amount of mutant SOD1 in the mitochondria. Dorfin reduced the levels of both cytosolic and mitochondrial mutant SOD1-EGFP fusion proteins that were expressed by Cyto-G93A and Cyto-G85R without organelle-oriented signals, whereas Dorfin did not affect the level of mutant SOD1-EGFP fusion protein that was expressed by Mito-G93A and Mito-G85R with mitochondrial localizing signals. The reduction in the level of

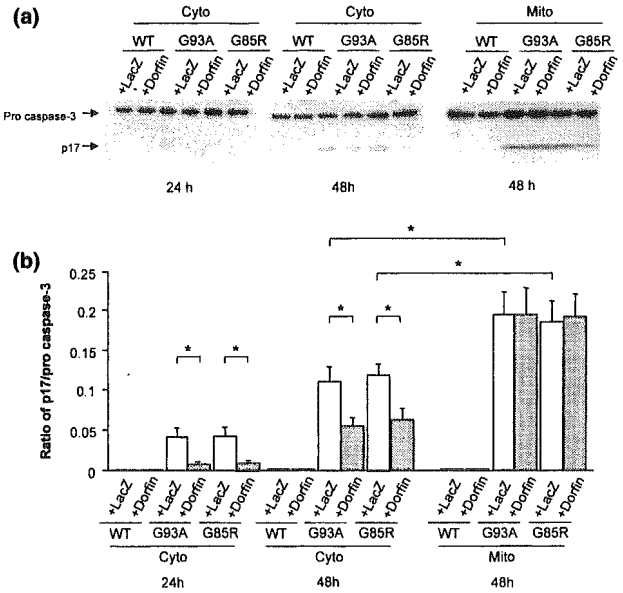

Fig. 8 Western blot analysis of caspase-3 activation. (a) Time course of activation of caspase-3. (b) Densitometric analysis of caspase-3 activation. The cells with Mito-G93A and Mito-G85R exhibited significantly more activation of caspase-3 than those with Cyto-G93A and Cyto-G85R. Dorfin significantly reduced the activation of caspase-3 induced by Cyto-G93A and Cyto-G85R, whereas it did not reduce that induced by Mito-SOD1. Values are mean ± SD ($n = 4$). $^*p < 0.05$ (two-way ANOVA with Tukey–Kramer post-hoc test).

mitochondrial SOD1-EGFP was observed earlier than that of total or cytosolic SOD1-EGFP. Moreover, Dorfin was present in the cytosol, not in the mitochondria. These findings indicated that the mitochondrial mutant SOD1 without organelle-oriented signals (Cyto-G93A and Cyto-G85R) might be translocated from the cytosol, and we suggest that Dorfin reduces the mitochondrial accumulation of mutant SOD1 by enhancing the degradation of mutant SOD1 in the cytosol through the ubiquitin–proteasomal pathway, thereby reducing the uptake of mutant SOD1 into the mitochondria.

Many reports have documented mitochondrial involvement in ALS and FALS. Mitochondrial degeneration with vacuolization or membrane disintegration in motor neurons is one of the earliest pathological findings in FALS Tg mice (Dal Canto and Gurney 1994; Wong *et al.* 1995; Hirano 1996; Kong and Xu 1998; Jaarsma *et al.* 2000; Higgins *et al.* 2003). Moreover, mitochondrial dysfunction such as altered calcium homeostasis (Carrì *et al.* 1997; Menzies *et al.* 2002b), decreased respiratory chain complex activity (Mattiazzi *et al.* 2002; Menzies *et al.* 2002a), alteration of mitochondria-related gene expression (Yoshihara *et al.* 2002) and an increase in reactive oxygen species (Beretta *et al.* 2003) have been reported in *in vitro* and *in vivo* models of FALS. Several studies have documented that SOD1, which has been considered a cytosolic enzyme, also exists in the mitochondrial intermembrane space (Okado-Matsumoto and Fridovich 2001; Sturtz *et al.* 2001; Higgins *et al.* 2002) and that the mitochondrial vacuoles are lined with mutant SOD1 in a FALS Tg mice model (Jaarsma *et al.* 2001; Higgins *et al.* 2003). Although the mitochondria-oriented vector we used here is designed to localize proteins to the mitochondrial matrix, we predict that SOD1-EGFP also exists in the mitochondrial intermembrane space through the process of its uptake into the mitochondrial matrix in our model, although were not able to confirm this. Recent studies also revealed that SOD1 in the mitochondria originates from the uptake of SOD1 in the cytosol (Sturtz *et al.* 2001; Okado-Matsumoto and Fridovich 2002; Field *et al.* 2003). At least our result provided enough evidence that Dorfin interacts with mutant SOD1 in the cytosol, not in the mitochondria. Thus we suggest that Dorfin indirectly reduces the mitochondrial accumulation of mutant SOD1 by reducing the uptake of mutant SOD1 into the mitochondria.

Previous studies demonstrated that the mitochondrial PCD pathway, cytochrome *c* release and subsequent caspase activation, might contribute to the motor neuron cell death in FALS (Durham *et al.* 1997; Martin 1999; Li *et al.* 2000; Pasinelli *et al.* 2000; Guégan *et al.* 2001; Kriz *et al.* 2002; Zhu *et al.* 2002). Thus, inhibiting the activation of the mitochondrial PCD pathway is potentially useful in the treatment of FALS. Methods for this include inhibition of cytochrome *c* release by minocycline (Zhu *et al.* 2002; Kriz *et al.* 2002), co-expression of bcl-2 (Lee *et al.* 2001) or X-chromosome-linked inhibitor of apoptosis protein (Ishigaki *et al.* 2002), and treatment with a broad caspase inhibitor zVAD-fmk (Pasinelli *et al.* 2000; Takeuchi *et al.* 2002a) or a caspase-9 specific inhibitor zLEHD-fmk (Takeuchi *et al.* 2002a). In this study, we demonstrated that Dorfin reduces the amount of mitochondrial mutant SOD1, attenuates the activation of the mitochondrial PCD pathway and prevents eventual neuronal cell death. It is therefore possible that reducing the amount of mutant SOD1 in the mitochondria may be adopted as a new therapeutic strategy for mutant SOD1-associated FALS.

Recent studies have suggested that some E3s, including Dorfin, act in a quality-control system to degrade cytosolic or transmembranous unfolded abnormal proteins (Moynihan *et al.* 1999; Fang *et al.* 2001; Meacham *et al.* 2001; Murata *et al.* 2001; Yoshida *et al.* 2002). The mitochondria also have a quality-control system that depends on mitochondria-specific molecular chaperones and ATPases associated with diverse cellular activities (AAA) proteases such as chaperonin 60 (Gottesman *et al.* 1997), mitochondrial heat-shock protein 70 (Savel'ev *et al.* 1998), and homologs of Lon, Yme1p, ClpP and ClpX (Wang *et al.* 1993; Suzuki *et al.* 1997; Langer 2000; Shah *et al.* 2000; Kang *et al.* 2002; Röttgers *et al.* 2003). A recent study documented that the accumulation of unfolded abnormal proteins in the mitochondria itself up-regulated the nuclear gene expression encoding mitochondrial-specific molecular chaperones (Zhao *et al.* 2002). Even though the mitochondria are able to dispose of abnormal proteins, they appear to have limited capacity to do this. They also seem to release death signals when abnormal proteins overflow their disposing capacity. Combination therapy such as Dorfin and mitochondria-specific molecular chaperones or AAA proteases thus seems more effective. Further investigations are needed to develop this therapeutic avenue.

There remains the problem of how the mutant SOD1 induces the mitochondrial PCD pathway. One of our previous studies revealed that bcl-2 family pro-apoptotic proteins, such as Bax, Bak, Bid, Bad and Bim, and other mitochondrial death signals such as apoptosis-inducing factor (AIF) and second mitochondria-derived activator of caspase (Smac) were not involved in the neuronal cell death in our model (Takeuchi *et al.* 2002a). Other studies have reported that translocation of Bax and cleavage of Bid were associated with neuronal cell death in the FALS Tg mouse model (Guégan *et al.* 2001; 2002), but there is a possibility that the surrounding environment of motor neurons such as astrocytes, microglia or dying neurons might have been affected in these models. Moreover, we have indicated that a non-apoptotic form of PCD might contribute to neuronal cell death through the mitochondrial PCD pathway in our model (Takeuchi *et al.* 2002a). Another report also mentioned that a non-apoptotic type of PCD acting through the mitochondrial PCD pathway might underlie mutant SOD1-related neurotoxicity (Guégan and Przedborski 2003). Further *in vivo*

investigations are needed to shed light on the mechanism of mutant SOD1-mediated neuronal cell death.

In this study we demonstrated that Dorfin, an E3 for mutant SOD1s, significantly reduced the level of mutant SOD1 in the mitochondria, attenuated the subsequent activation of the mitochondrial PCD pathway and prevented eventual neuronal cell death in a neuronal cell model of FALS. Reducing the accumulation of mutant SOD1 in the mitochondria may have an important place in the therapeutic strategy for mutant SOD1-associated FALS, and Dorfin may play a key role in this.

Acknowledgements

We are grateful to Dr Keiji Tanaka (Department of Molecular Oncology, The Tokyo Metropolitan Institute of Medical Science) for his helpful comments. This work was supported by grants from the Ministry of Health, Labor and Welfare of Japan, and a Center of Excellence grant from the Ministry of Education, Culture, Sports, Science and Technology of Japan.

References

Ardley H. C., Tan N. G. S., Rose S. A., Markham A. F. and Robinson P. A. (2001) Features of the Parkin/Ariadne-like ubiquitin ligase, HHARI, that regulate its interaction with the ubiquitin-conjugating enzyme, UbcH7. *J. Biol. Chem.* **276**, 19640–19647.

Beretta S., Sala G., Mattavelli L., Ceresa C., Casciati A., Ferri A., Carr ı M. T. and Ferrarese C. (2003) Mitochondrial dysfunction due to mutant copper/zinc superoxide dismutase associated with amyotrophic lateral sclerosis is reversed by *N*-acetylcysteine. *Neurobiol. Dis.* **13**, 213–221.

Carrì M. T., Ferri A., Battistoni A., Famhy L., Gabbianelli R., Poccia F. and Rotilio G. (1997) Expression of a Cu,Zn superoxide dismutase typical of familial amyotrophic lateral sclerosis induces mitochondrial alteration and increase of cytosolic Ca^{2+} concentration in transfected neuroblastoma SH-SY5Y cells. *FEBS Lett.* **414**, 365–368.

Dal Canto M. C. and Gurney M. E. (1994) Development of central nervous system pathology in a murine transgenic model of human amyotrophic lateral sclerosis. *Am. J. Pathol.* **145**, 1271–1279.

Durham H. D., Roy J., Dong L. and Figlewic Z. D. A. (1997) Aggregation of mutant Cu/Zn superoxide dismutase proteins in a culture model of ALS. *J. Neuropathol. Exp. Neurol.* **56**, 523–530.

Fang S., Ferrone M., Yang C., Jensen J. P., Tiwari S. and Weissman A. M. (2001) The tumor autocrine motility factor receptor, gp78, is a ubiquitin protein ligase implicated in degradation from the endoplasmic reticulum. *Proc. Natl Acad. Sci. USA* **98**, 14422–14427.

Field L. S., Furukawa Y., O'Halloran T. V. and Culotta V. C. (2003) Factors controlling the uptake of yeast Cu/Zn superoxide dismutase into mitochondria. *J. Biol. Chem.* **278**, 28052–28059.

Gottesman S., Wickner S. and Maurizi M. R. (1997) Protein quality control: triage by chaperones and proteases. *Genes Dev.* **11**, 815–823.

Guégan C. and Przedborski S. (2003) Programmed cell death in amyotrophic lateral sclerosis. *J. Clin. Invest.* **111**, 153–161.

Guégan C., Vila M., Rosoklija G., Hays A. P. and Przedborski S. (2001) Recruitment of the mitochondrial-dependent apoptotic pathway in amyotrophic lateral sclerosis. *J. Neurosci.* **21**, 6569–6576.

Guégan C., Vila M., Teissman P., Chen C., Onténiente B., Li M., Friedlander R. M. and Przedborski S. (2002) Instrumental activation of Bid by caspase-1 in a transgenic mouse model of ALS. *Mol. Cell. Neurosci.* **20**, 553–562.

Higgins C. M., Jung C., Ding H. and Xu Z. (2002) Mutant Cu,Zn superoxide dismutase that causes motoneuron degeneration is present in mitochondria in the CNS. *J. Neurosci.* **22 RC215**.

Higgins C. M. J., Jung C. and Xu Z. (2003) ALS-associated mutant SOD1G93A causes mitochondrial vacuolation by expansion of the intermembrane space and by involvement of SOD1 aggregation and peroxisomes. *BMC Neurosci.* **4**, 16–29.

Hirano A. (1996) Neuropathology of ALS: an overview. *Neurology* **47**, S63–S66.

Ishigaki S., Liang Y., Yamamoto M., Niwa J., Ando Y., Yoshihara T., Takeuchi H., Doyu M. and Sobue G. (2002) X-linked inhibitor of apoptosis protein is involved in mutant SOD1-mediated neuronal degeneration. *J. Neurochem.* **82**, 576–584.

Jaarsma D., Haasdijk E. D., Grashorn J. A. C., Hawkins R., van Duijn W., Verspaget H. W., London J. and Holstege J. C. (2000) Human Cu/Zn superoxide dismutase (SOD1) overexpression in mice causes mitochondrial vacuolization, axonal degeneration, and premature motoneuron death and accelerates motoneuron disease in mice expressing a familial amyotrophic lateral sclerosis mutant SOD1. *Neurobiol. Dis.* **7**, 623–643.

Jaarsma D., Rognoni F., van Duijn W., Verspaget H. W., Haasdijk E. D. and Holstege J. C. (2001) CuZn superoxide dismutase (SOD1) accumulates in vacuolated mitochondria in transgenic mice expressing amyotrophic lateral sclerosis-linked SOD1 mutations. *Acta Neuropathol.* **102**, 293–305.

Kang S. G., Ortega J., Singh S. K., Wang N., Huang N., Steven A. C. and Maurizi M. R. (2002) Functional proteolytic complexes of the human mitochondrial ATP-dependent protease, hClpXP. *J. Biol. Chem.* **277**, 21095–21102.

Kong J. and Xu Z. (1998) Massive mitochondrial degeneration in motor neurons triggers the onset of amyotrophic lateral sclerosis in mice expressing a mutant SOD1. *J. Neurosci.* **18**, 3241–3250.

Kriz J., Nguyen M. D. and Julien J. P. (2002) Minocycline slows disease progression in a mouse model of amyotrophic lateral sclerosis. *Neurobiol. Dis.* **10**, 268–278.

Langer T. (2000) AAA proteases: cellular machines for degrading membrane proteins. *Trends Biochem. Sci.* **25**, 247–251.

Lee M. H., Hyun D.-H., Halliwell B. and Jenner P. (2001) Effect of overexpression of wild-type and mutant Cu/Zn-superoxide dismutases on oxidative stress and cell death induced by hydrogen peroxide, 4-hydroxynonenal or serum deprivation: potentiation of injury by ALS-related mutant superoxide dismutases and protection by Bcl-2. *J. Neurochem.* **78**, 209–220.

Li M., Ona V. O., Guégan C. *et al.* (2000) Functional role of caspase-1 and caspase-3 in an ALS transgenic mouse model. *Science* **288**, 335–339.

Martin L. J. (1999) Neuronal death in amyotrophic lateral sclerosis is apoptosis: possible contribution of a programmed cell death mechanism. *J. Neuropathol. Exp. Neurol.* **58**, 459–471.

Mattiazzi M., D'Aurelio M., Gajewski C. D., Martushova K., Kiaei M., Beal M. F. and Manfredi G. (2002) Mutated human SOD1 causes dysfunction of oxidative phosphorylation in mitochondria of transgenic mice. *J. Biol. Chem.* **277**, 29626–29633.

Meacham G. C., Patterson C., Zhang W., Younger J. M. and Cyr D. M. (2001) The Hsc70 co-chaperone CHIP targets immature CFTR for proteasomal degradation. *Nat. Cell Biol.* **3**, 100–105.

Menzies F. M., Cookson M. R., Taylor R. W., Turnbull D. M., Chrzanowska-Lightowlers Z. M., Dong L., Figlewicz D. A. and Shaw P. J. (2002a) Mitochondrial dysfunction in a cell culture model of familial amyotrophic lateral sclerosis. *Brain* **125**, 1522–1533.

Menzies F. M., Ince P. G. and Shaw P. J. (2002b) Mitochondrial involvement in amyotrophic lateral sclerosis. *Neurochem. Int.* **40**, 543–551.

Moynihan T. P., Ardley H. C., Nuber U., Rose S. A., Jones P. F., Markham A. F., Scheffner M. and Robinson P. A. (1999) The ubiquitin-conjugating enzymes UbcH7 and UbcH8 interact with RING finger/IBR motif-containing domains of HHARI and H7-AP1. *J. Biol. Chem.* **274**, 30963–30968.

Murata S., Minami Y., Minami M., Chiba T. and Tanaka K. (2001) CHIP is a chaperone-dependent E3 ligase that ubiquitylates unfolded protein. *EMBO Report* **2**, 1133–1138.

Niwa J., Ishigaki S., Doyu M., Suzuki T., Tanaka K. and Sobue G. (2001) A novel centrisomal RING-finger protein, Dorfin, mediates ubiquitin ligase activity. *Biochem. Biophys. Res. Commun.* **281**, 706–713.

Niwa J., Ishigaki S., Hishikawa N., Yamamoto M., Doyu M., Murata S., Tanaka K., Taniguchi N. and Sobue G. (2002) Dorfin ubiquitylates mutant SOD1 and prevents mutant SOD1-mediated neurotoxicity. *J. Biol. Chem.* **277**, 36793–36798.

Okado-Matsumoto A. and Fridovich I. (2001) Subcellular distribution of superoxide dismutase (SOD) in rat liver. *J. Biol. Chem.* **276**, 38388–38393.

Okado-Matsumoto A. and Fridovich I. (2002) Amyotrophic lateral sclerosis: a proposed mechanism. *Proc. Natl Acad. Sci. USA* **99**, 9010–9014.

Pasinelli P., Houseweart M. K., Brown R. H. Jr and Cleveland D. W. (2000) Caspse-1 and -3 are sequentially activated in motor neuron death in Cu,Zn superoxide dismutase-mediated familial amyotrophic lateral sclerosis. *Proc. Natl Acad. Sci. USA* **97**, 13901–13906.

Raoul C., Estévez A. G., Nishimune H., Cleveland D. W., deLapeyrière O., Henderson C. E., Haase G. and Pettmann B. (2002) Motoneuron death triggered by a specific pathway downstream of Fas; potentiation by ALS-linked SOD1 mutations. *Neuron* **35**, 1067–1083.

Rosen D. R., Siddique T., Patterson D. *et al.* (1993) Mutations in Cu/Zn superoxide dismutase gene are associated with familial amyotrophic lateral sclerosis. *Nature* **362**, 59–62.

Röttgers K., Zufall N., Guiard B. and Voos W. (2003) The ClpB homolog Hsp78 is required for the efficient degradation of proteins in the mitochondrial matrix. *J. Biol. Chem.* **277**, 45829–45837.

Savel'ev A. S., Novikova L. A., Kovaleva I. E., Luzikov V. N., Neupert W. and Langer T. (1998) ATP-dependent proteolysis in mitochondria. *J. Biol. Chem.* **273**, 20596–20602.

Shah Z. H., Hakkaart G. A. J., Arku B., de Jong L., van der Spek H., Grivell L. A. and Jacobs H. T. (2000) The human homologue of the yeast mitochondrial AAA metalloprotease Yme1p complements a yeast *yme1* disruptant. *FEBS Lett.* **478**, 267–270.

Sturtz L. A., Diekert K., Jensen L. T., Lill R. and Culotta V. C. (2001) A fraction of yeast Cu,Zn-superoxide dismutase and its metallochaperone, CCS, localize to the intermembrane space of mitochondria. *J. Biol. Chem.* **276**, 38084–38089.

Suzuki C. K., Rep M., van Dijl J. M., Suda K., Grivell L. A. and Schatz G. (1997) ATP-dependent proteases that also chaperone protein biogenesis. *Trends Biochem. Sci.* **22**, 118–123.

Takeuchi H., Kobayashi Y., Ishigaki S., Doyu N. and Sobue G. (2002a) Mitochondrial localization of mutant superoxide dismutase 1 triggers caspase-dependent cell death in a cellular model of familial amyotrophic lateral sclerosis. *J. Biol. Chem.* **277**, 50966–50972.

Takeuchi H., Kobayashi Y., Yoshihara T., Niwa J., Doyu M., Ohtsuka K. and Sobue G. (2002b) Hsp70 and Hsp40 improve neurite outgrowth and suppress intracytoplasmic aggregate formation in cultured neuronal cells expressing mutant SOD1. *Brain Res.* **949**, 11–22.

Wang N., Gottesman S., Willingham M. C., Gottesman M. M. and Maurizi M. R. (1993) A human mitochondrial ATP-dependent protease that is highly homologous to bacterial Lon protease. *Proc. Natl Acad. Sci. USA* **90**, 11247–11251.

Wong P. C., Pardo C. A., Borchelt D. R., Lee M. K., Copeland N. G., Jenkins N. A., Sisodia S. S., Cleveland D. W. and Price D. L. (1995) An adverse property of a familial ALS-linked SOD1 mutation causes motor neuron disease characterized by vacuolar degeneration of mitochondria. *Neuron* **14**, 1105–1116.

Yim M. B., Kang J. H., Yim H. S., Kwak H. S., Chock P. B. and Stadtman E. R. (1996) A gain-of-function of an amyotrophic lateral sclerosis-associated Cu,Zn-superoxide dismutase mutant: an enhancement of free radical formation due to a decrease in K_m for hydrogen peroxide. *Proc. Natl Acad. Sci. USA* **93**, 5709–5714.

Yoshida Y., Chiba T., Tokunaga F. *et al.* (2002) E3 ubiquitin ligase that recognizes sugar chains. *Nature* **418**, 438–442.

Yoshihara T., Ishigaki S., Yamamoto M., Liang Y., Niwa J., Takeuchi H., Doyu M. and Sobue G. (2002) Differential expression of inflammation- and apoptosis-related genes in spinal cords of a mutant SOD1 transgenic mouse model of familial lateral sclerosis. *J. Neurochem.* **80**, 158–167.

Zhao Q., Wang J., Levichkin I. V., Stasinopoulos S., Ryan M. T. and Hoogenraad N. J. (2002) A mitochondrial specific stress response in mammalian cells. *EMBO J.* **21**, 4411–4419.

Zhu S., Stavrovskaya I. G., Drozda M. *et al.* (2002) Minocycline inhibits cytochrome *c* release and delays progression of amyotrophic lateral sclerosis. *Nature* **417**, 74–78.

PAPER

Multiple regional ^{1}H-MR spectroscopy in multiple system atrophy: NAA/Cr reduction in pontine base as a valuable diagnostic marker

H Watanabe, H Fukatsu, M Katsuno, M Sugiura, K Hamada, Y Okada, M Hirayama, T Ishigaki, G Sobue

J Neurol Neurosurg Psychiatry 2004;75:103–109

See end of article for authors' affiliations

Correspondence to: Gen Sobue, MD, Department of Neurology, Nagoya University Graduate School of Medicine, Nagoya 466-8550 Japan; sobueg@med.nagoya-u.ac.jp

Received 20 December 2002
In revised form 31 March 2003
Accepted 17 May 2003

Objective: We performed ^{1}H-MR spectroscopy (^{1}H-MRS) on multiple brain regions to determine the metabolite pattern and diagnostic utility of ^{1}H-MRS in multiple system atrophy (MSA).
Methods: Examining single voxels at 3.0 T, we studied metabolic findings of the putamen, pontine base, and cerebral white matter in 24 MSA patients (predominant cerebellar ataxia (MSA-C), n=13), parkinsonism (MSA-P), n=11), in 11 age and duration matched Parkinson's disease patients (PD) and in 18 age matched control subjects.
Results: The *N*-acetylaspartate to creatine ratio (NAA/Cr) in MSA patients showed a significant reduction in the pontine base ($p<0.0001$) and putamen ($p=0.02$) compared with controls. NAA/Cr in cerebral white matter also tended to decline in long standing cases. NAA/Cr reduction in the pontine base was prominent in both MSA-P ($p<0.0001$) and MSA-C ($p<0.0001$), and putaminal NAA/Cr reduction was significant in MSA-P ($p=0.009$). It was also significant in patients who were in an early phase of their disease, and in those who showed no ataxic symptoms or parkinsonism, or did not show any MRI abnormality of the "hot cross bun" sign or hyperintense putaminal rims. NAA/Cr in MSA-P patients was significantly reduced in the pontine base ($p=0.001$) and putamen ($p=0.002$) compared with PD patients. The combined ^{1}H-MRS in the putamen and pontine base served to distinguish patients with MSA-P from PD more clearly.
Conclusions: ^{1}H-MRS showed widespread neuronal and axonal involvement in MSA. The NAA/Cr reduction in the pontine base proved highly informative in the early diagnosis of MSA prior to MRI changes and even before any clinical manifestation of symptoms.

Multiple system atrophy (MSA) is a sporadically occurring neurodegenerative disease that presents parkinsonism, cerebellar ataxia, autonomic failure, and pyramidal signs of varying severity during the course of illness.[1–3] Neuropathological findings consist of a varying neuronal loss, gliosis, and demyelination with widespread regional involvement, particularly including the striatonigral, olivopontocerebellar, and autonomic nervous systems.[4–6] The tempo and progression of multiple system involvement vary widely among individual MSA patients and have been closely related to both functional deterioration and prognosis by clinical evaluation.[7] Thus, assessing the multi-regional involvement in MSA is essential for accurate diagnosis, counselling of patients and families, optimal management of symptoms, and the usefulness of future therapeutic trials.

Proton magnetic resonance spectroscopy (^{1}H-MRS) is a valuable non-invasive MR technique for monitoring brain metabolism in vivo.[8–18] The major peaks of the ^{1}H-MRS spectrum, corresponding to *N*-acetylaspartate (NAA), creatine (Cr), and choline (Cho) containing phospholipids, have been used to evaluate neuronal loss and active myelin breakdown. The ratio of NAA to Cr (NAA/Cr) is considered a metabolic marker reflecting the functional status of neurones and axons in the brain, with a decrease indicating neuronal or axonal loss or dysfunction. Previous studies using ^{1}H-MRS in MSA with predominant parkinsonism (MSA-P) reported a significant NAA/Cr reduction in the striatum compared with Parkinson's disease (PD) patients and normal subjects.[11–14] However, the pontine base and cerebral white matter, which are also pathologically involved in MSA, have not been fully assessed by ^{1}H-MRS. Recent technical innovations have permitted ^{1}H-MRS at higher magnetic field strengths.[19–21] Multi-regional data can be obtained from single voxel ^{1}H-MRS within a short examination time with increasing signal to noise ratio (SNR).

Our purpose was to assess the extent of multiple system involvement in patients with MSA by using multiple regional single voxel ^{1}H-MRS including the putamen, pontine base, and cerebral white matter (CWM), and to further assess the diagnostic value of the regional ^{1}H-MRS.

METHODS

All patients and control subjects gave written informed consent. The MR protocol was approved by the Ethics Committee of the Nagoya University School of Medicine. Twenty four patients with MSA (12M, 12F; mean (SD) age 61 (7) years old), 11 patients with PD (5M, 6F; 63 (9) years old), and 18 control subjects with no history of any neurological disease (10M, 8F; 59 (7) years old) were studied. No significant differences in male to female ratio or age were noted among the three groups. The duration from initial

Abbreviations: Cho, choline; Cr, creatine; CWM, cerebral white matter; HCB, "hot cross bun"; HPR, hyperintense rim; MRI, magnetic resonance imaging; MRS, magnetic resonance spectroscopy; MSA, multiple system atrophy; MSA-C, multiple system atrophy with cerebellar ataxia predominant; MSA-P, multiple system atrophy with parkinsonism predominant; NAA, *N*-acetylaspartate; PD, Parkinson's disease; SNR, signal to noise ratio; VOI, volume of interest.

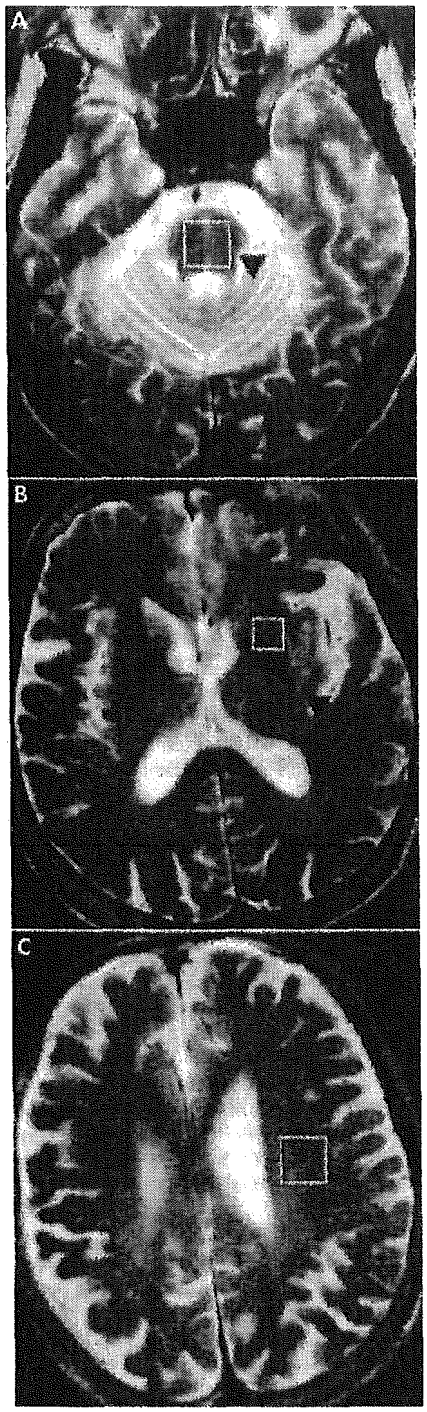

Figure 1 Location of volumes of interest are shown by squares in the pontine base (A), putamen (B), and white matter of the frontal lobe (C). Additionally, in these images, an HCB sign is present in the pons (A), as is a hyperintense putaminal rim (B). Axial T2 weighted images (3.0 T; TR: 3970, TE: 80), with respective findings are indicated by arrowheads.

symptoms to MRI and MRS evaluation also showed no differences between MSA and PD patients (MSA; 3.7 (2.4) years; PD; 4.4 (2.2) years, $p>0.4$). Diagnoses of all MSA and PD patients were "probable" according to established diagnostic criteria.[3 22] As for subtypes of MSA, cerebellar dysfunction (MSA-C) predominated in 13 patients and parkinsonism (MSA-P) in 11. We classified patients into two groups according to the presence of parkinsonian signs in MSA, based on the consensus statement for MSA diagnosis. Patients with bradykinesia plus at least one sign of either rigidity, postural instability, or tremor were considered to manifest parkinsonism and designated as "parkinsonism+", while others were taken to be "parkinsonism−". As for cerebellar dysfunction, patients with gait ataxia plus at least one sign of ataxic dysarthria, limb ataxia, or sustained gaze evoked nystagmus were considered "ataxia+", and others as "ataxia−" based on the consensus criteria.[3] Six of nine MSA-P patients and all PD patients were taking medication for parkinsonism (benserazide/levodopa 25/100 mg, or carbidopa/levodopa 10/100 mg, two or three times daily). All PD patients showed a good response to treatment.

MRI and ^{1}H-MRS were performed with a 3.0 T system (Bruker, Ettlingen, Germany) using a standard head coil with circular polarisation. The imaging protocol consisted of sagittal T1 weighted spin echo sequences (repetition time (TR), 460 ms; echo time (TE), 14 ms) and transverse T2 weighted sequences (TR, 3970 ms; TE, 80 ms). Slice thickness was 6 mm with a 1.2 mm gap and a 512×384 matrix. We evaluated whether a "hot cross bun" (HCB) sign was present in the pons and whether the putamen showed a hyperintense rim (HPR), according to the criteria described in previous reports (fig 1A, B).[7 23-26] The spectroscopic volume of interest (VOI) was placed in the pontine base (2.2 to 3.4 cm^3), the putamen (1 cm^3), and the CWM (3.4 cm^3; fig 1A to C). Voxel size was chosen to be as small as possible while maintaining an acceptable SNR in order to minimise the partial volume effect. Care was taken not to incorporate cerebrospinal fluid spaces within a VOI. The VOI in the putamen was placed on the more affected side, and the frontal lobe VOI was ipsilateral to the putaminal VOI. ^{1}H-MR spectra were acquired using a point resolved spectroscopy sequence with chemical shift selective water suppression. Spectral parameters were as follows: TR: 2000 ms; TE: 30 ms; averages: 256 in the putamen, and 64 each in the centrum semiovale and pons; data points: 1024. A shimming procedure focused on the water signal was performed to obtain a uniform and homogenous magnetic field. After Fourier transformation and zero order phase correction, relative metabolite concentrations for NAA at 2.0 ppm, Cr at 3.0 ppm, and Cho at 3.2 ppm were determined by Lorentzian curve fitting of the corresponding resonance in the frequency spectra. The baseline was corrected for purposes of data presentation. From these data, the metabolite ratios NAA/Cr, and Cho/Cr were determined as semiquantitative values. Post-procedural processing was performed by the same radiologist (HF). All preconditioning, spectroscopic measurements, and processing were performed with Paravision 2.01 software (Bruker). Total examination time including MRI and ^{1}H-MRS was <1 hour. One MSA-C patient with severe pontine atrophy was excluded because a good pontine spectrum could not be obtained.

Values obtained were entered into a database for further statistical analysis. The Mann-Whitney U test and the Kruskal-Wallis test for nonparametric statistics were performed as appropriate. When the Kruskal-Wallis test indicated differences among groups, in a multiple comparison analysis, Scheffé's test was used to identify which group differences accounted for the significant p value. Relationships of NAA/Cr reduction to duration of illness were analysed using Pearson's correlation coefficient. Calculations were performed using the Stat View statistical software package (Abacus Concepts, Berkeley, CA, USA). Statistical significance was defined as $p<0.05$.

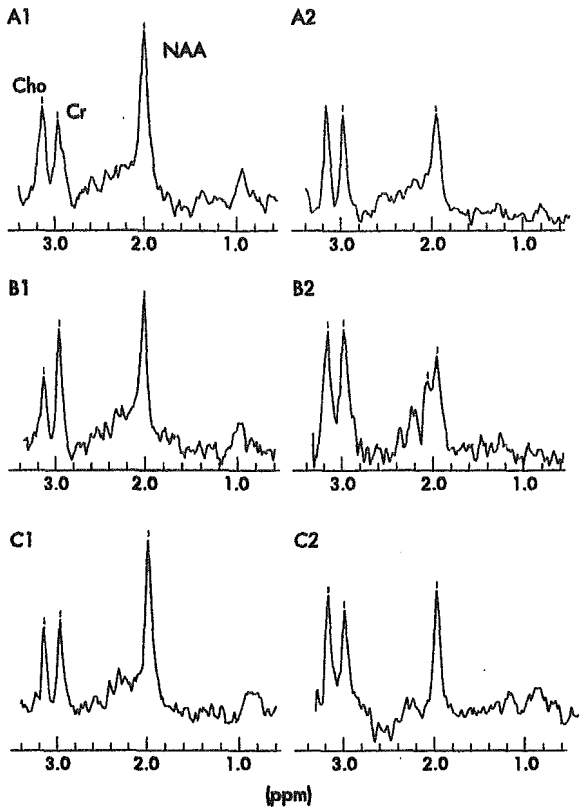

Figure 2 Representative ^{1}H-MRS spectra from control and MSA subjects. A1, B1, and C1 represent spectra from a control subject's pontine base, putamen, and cerebral white matter, respectively. A2, B2, and C2 represent spectra from those same three regions in an MSA patient. NAA, *N*-acetylaspartate; Cho, choline; Cr, creatine; MSA, multiple system atrophy; CWM, cerebral white matter.

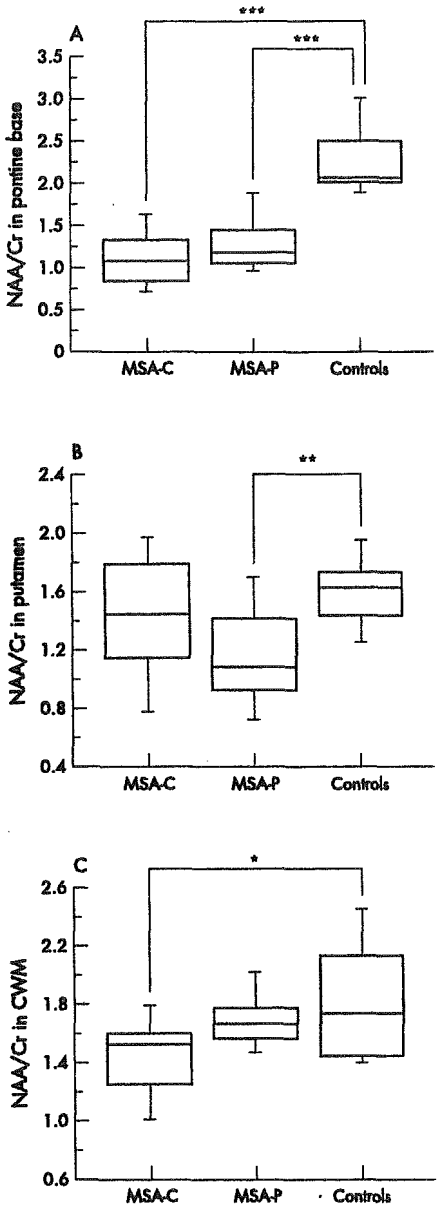

Figure 3 Box and whisker plot of the NAA/Cr ratio. Horizontal lines indicate median values. Boxes extend from the 25th to the 75th percentile. A, B, and C respectively show NAA/Cr in the pontine base, putamen, and cerebral white matter, comparing MSA-C, MSA-P, and control subjects. *p=0.02, **p=0.009, and ***p<0.0001 by Scheffé's test, respectively. NAA, *N*-acetylaspartate; Cr, creatine; Cho, choline containing component; MSA-C, multiple system atrophy with cerebellar ataxia predominant; MSA-P, multiple system atrophy with parkinsonism predominant.

RESULTS

Widespread NAA/Cr reduction in MSA in multiple regional ^{1}H-MRS

A representative MSA patient (fig 2) showed a marked reduction of the NAA peak in the pontine base, putamen, and cerebral white matter compared with controls. NAA/Cr was significantly reduced in the pontine base of MSA patients ($p<0.0001$) and in the putamen ($p=0.02$) compared with controls. MSA patients also showed a lower NAA/Cr in cerebral white matter than controls, but this difference was not statistically significant ($p=0.12$). Cho/Cr was only slightly increased in MSA, and no significant differences were found among the three groups for the pontine base, putamen, and CWM.

Prominent NAA/Cr reduction in pontine base in both MSA-C and MSA-P

Significant reductions of NAA/Cr were evident in the pontine base, putamen, and CWM in MSA-C and MSA-P compared with controls (fig 3A–C). MSA-C patients showed a significant reduction of NAA/Cr in the pontine base ($p<0.0001$) and CWM ($p=0.02$), but not in the putamen. MSA-P patients showed a significant reduction of NAA/Cr in the pontine base ($p<0.0001$) and putamen ($p=0.009$) but not in the CWM. These observations indicate that the NAA/Cr reduction in the pontine base was significant in both MSA-C and MSA-P. Cho/Cr was not changed in MSA-P or MSA-C compared with controls.

Relation of NAA/Cr reduction in pontine base with disease phase, motor symptoms and MRI abnormalities in MSA

In terms of disease duration, the NAA/Cr reduction was most significant in the pontine base of patients with MSA even in an early phase of illness (fig 4). A tendency toward an inverse

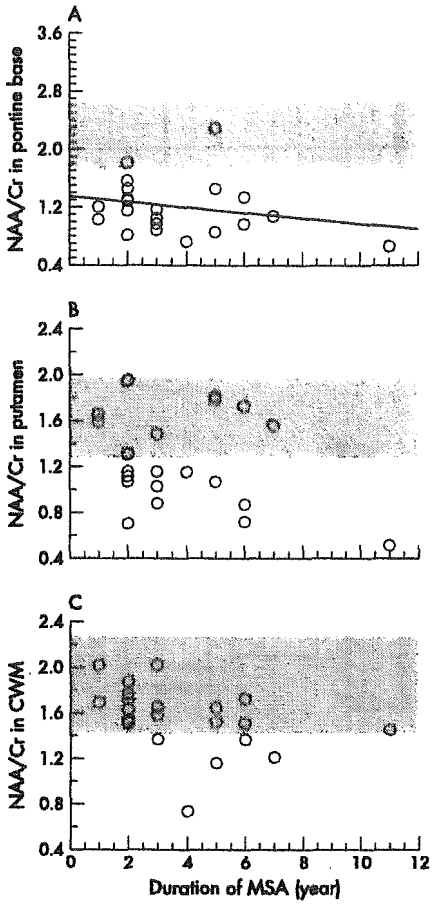

Figure 4 Correlation with duration of MSA of individual NAA/Cr ratios in the pontine base (A), putamen (B), and cerebral white matter (C). The shaded area corresponds to the mean (SD) of NAA/Cr in control subjects. NAA, *N*-acetylaspartate; Cr, creatine; CWM, cerebral white matter; MSA, multiple system atrophy.

relationship between disease duration and NAA/Cr in the three regions was observed, but did not attain significance (pontine base: $r = -0.24$, $p = 0.29$; putamen: $r = -0.32$, $p = 0.14$; CWM: $r = -0.41$, $p = 0.06$). NAA/Cr in the pontine base was significantly reduced compared with controls even in patients who did not show ataxic symptoms ($p = 0.0006$, fig 5A-1). However, NAA/Cr in the putamen and white matter was not reduced in patients with ataxia (fig 5B-1, C-1). NAA/Cr in the putamen was markedly decreased in MSA patients with parkinsonism ($p = 0.02$, Fig 5B-2), whereas patients without it exhibited no significant reduction compared with controls. NAA/Cr reduction in the pontine base, on the other hand, was significant ($p<0.0001$) irrespective of parkinsonism (Fig 5A-2).

The MRI revealed the HCB sign in the pontine base in eleven MSA patients (46%) and the HPR sign in six (25%). A significant reduction of NAA/Cr was seen in the pontine base even in patients without ($p<0.0001$) as well as in those with an HCB sign ($p<0.0001$; fig 5A-3). In the putamen and cerebral white matter, NAA/Cr values did not show any significant difference irrespective of the HCB sign (fig 5B-3, C-3). Moreover, NAA/Cr significantly decreased in the pontine base in patients both with and without HPR (fig 5A-4). NAA/Cr in the putamen and cerebral white matter did not show any significant differences irrespective of HPR signs (fig 5B-4, C-4). Cho/Cr had no significant relationship to ataxic, parkinsonism, or MRI abnormalities.

NAA/Cr in pontine base in MSA-P and PD

NAA/Cr reduction in the pontine base was highly significant in patients with MSA-P compared with both controls and PD ($p<0.0001$, $p = 0.001$; fig 6A). NAA/Cr in the putamen in MSA-P patients also showed a significant decrease compared with both controls and PD ($p = 0.003$, $p = 0.002$; fig 6B). No significant differences in NAA/Cr were noted in cerebral white matter between MSA-P and PD. These data indicate that the NAA/Cr reduction in the pontine base is a valuable marker to discriminate MSA-P from PD. In addition, combining individual NAA/Cr values for the pontine base and putamen further reduced the overlap between MSA-P and PD (fig 6D), suggesting that a combined assessment of the pontine base and putamen was more effective in discriminating between MSA-P and PD than individual area assessments. Cho/Cr did not display any significant changes in the pontine base, putamen or cerebral white matter.

DISCUSSION

We demonstrated widespread NAA/Cr reduction in the pontine base, putamen and in some cases, in the cerebral hemisphere, but no significant Cho/Cr alteration in patients with MSA using localised ^{1}H-MRS at 3.0 T. In this study, absolute metabolite concentrations were not measured. However, the specific conditions that may change the total Cr signal, such as trauma, hyperosmolar conditions, hypoxia, stroke, and tumours, were not included. Age was matched among MSA, PD, and control groups. Moreover, quantitative studies did not show significant Cr changes between MSA patients and control subjects.[11 16] Thus, the reduction of the NAA/Cr ratio in the present study can be considered due to a selective decrease in NAA levels.

NAA has been immunohistochemically demonstrated to localise almost exclusively within neurones and axons,[27 28] but some in vitro studies have also detected NAA expression in mature, immature, and undifferentiated oligodendrocytes.[29 30] Nevertheless, according to a recent study, in vivo MRS measurements of NAA remain axon specific, with no oligodendrocytes, nonproliferating oligodendrocyte progenitor cells, or myelin contributing to detectable NAA in the mature CNS.[31] This result supports the view that the widespread NAA/Cr reductions observed in this study ultimately reflect widespread neuronal and axonal involvement in MSA, although oligodendrocytes might influence the NAA levels to some degree.

The striking observation in this study is that the NAA/Cr reduction in the pontine base was the most significant among the three regions examined. That reduction was detected in the early phase of illness even in patients with no symptoms of ataxia or parkinsonism, or in patients without MRI abnormality of the HCB sign. Moreover, the pontine NAA/Cr reduction was significant even in MSA-P patients. In addition, NAA/Cr reductions in the pontine base were seen even in patients with no HPR sign in the lateral putamen. These observations suggest that NAA/Cr reduction in the pontine base is an accurate diagnostic marker for MSA even in patients in an early stage and a pre-symptomatic phase of ataxia or parkinsonism. The diagnostic focus of ^{1}H-MRS in MSA has been on the putamen,[11–14] whereas our results unequivocally demonstrated that MRS abnormality can be detected sooner and more universally in the pontine base than in the putamen in the course of the disease. The question is why a significant NAA/Cr reduction can be detected more readily in the pontine base than in the putamen. One reason may be that neuroaxonal degeneration

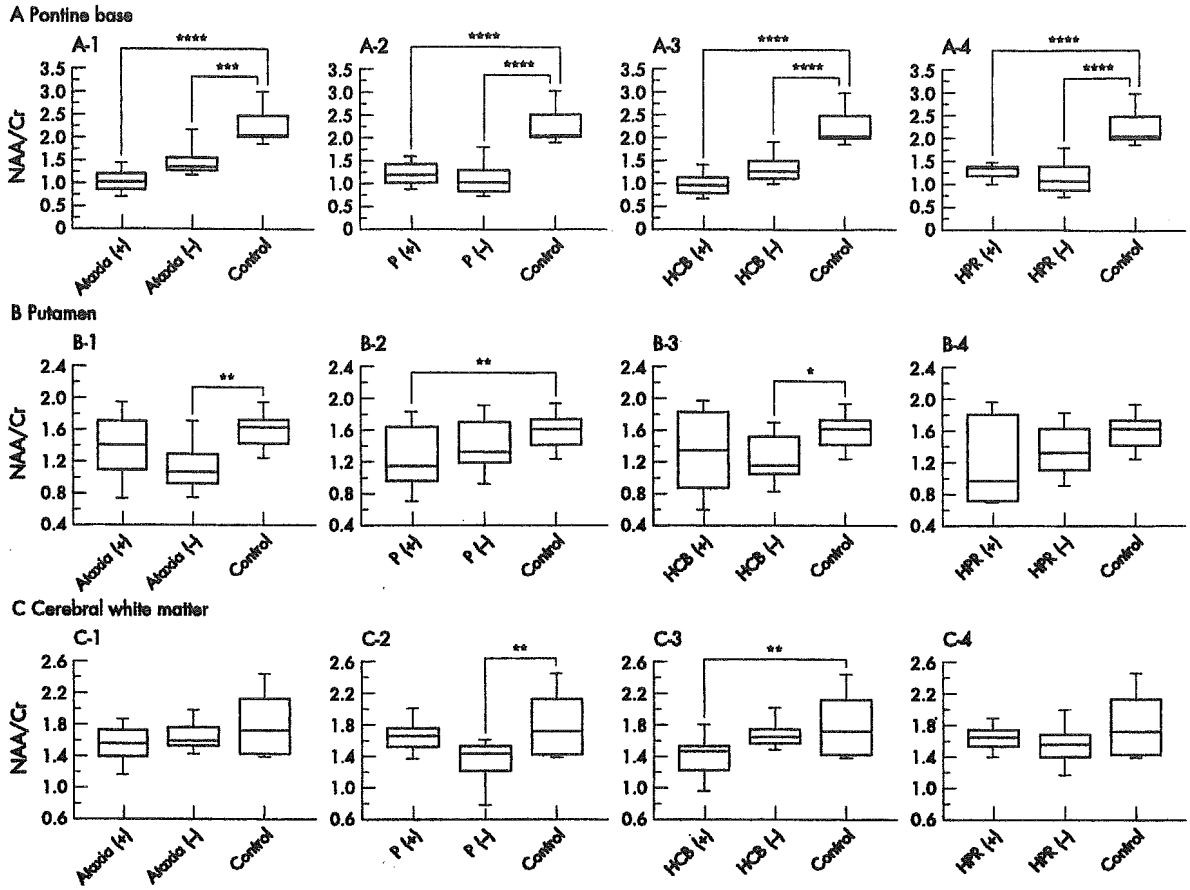

Figure 5 NAA/Cr in the pontine base (A), putamen (B), and cerebral white matter (C) for MSA patients classified in terms of clinical features of ataxia (+ or −; A-1, B-1, C-1), parkinsonism (P; + or −; A-2, B-2, C-2), HCB on MRI (+ or −; A-3, B-3, C-3), and hyperintense putaminal rim (HPR) on MRI (+ or −; A-4, B-4, C-4). +, Presence; −, absence. *p=0.047, **p=0.02, ***p=0.0006, and ****p<0.0001 by Scheffé's test, respectively. NAA, N-acetylaspartate; Cr, creatine; MSA, multiple system atrophy; CWM, cerebral white matter.

in the pons would be more extensive than in the putamen. As the pontine base consists of the axons and neurones specifically involved in MSA (for example fibres of cerebellar inflow and outflow, corticospinal tracts and transverse pontine tracts), subclinical involvement of such fibres could be detected as a reduction of NAA/Cr. Furthermore, because, as we demonstrated previously, MSA-C is significantly more prevalent in Japan than MSA-P, compared with white populations in the western countries,[7] the cerebellar pontine system should be more profoundly involved in Japanese MSA patients. A second possibility is that the volume effect due to putaminal atrophy would ultimately include the neighbouring normal tissues in the VOI of the MRS, influencing the degree of the NAA/Cr reduction. As atrophy of the putamen is severe in certain patients, the size of the VOI is a limiting factor in ^{1}H-MRS for maintaining an acceptable SNR. Such volume effects due to putaminal atrophy can result in conflicting data. Clarke and Lowry reported an absence of significant reductions in basal ganglionic NAA/Cr in MSA,[16] precluding the use of NAA/Cr reductions in the striatum for differential diagnosis.[16] Disease duration in their patients averaged 7.9 years.[16] In contrast, mean disease duration in other reports showing significant NAA/Cr reductions in the striatum of MSA patients ranged from 3.2 to 4.5 years,[11–14] similar to the duration in our patients. Because, with longer duration, putaminal atrophy in patients with MSA-P becomes more severe, discrepancies could be explained by differences in putaminal atrophy that can profoundly influence ^{1}H-MRS results. By avoiding this volume effect, MRS for the pontine base would provide a more accurate diagnostic marker.

Discriminating clearly between MSA-P and PD has long been a diagnostic problem from both therapeutic and prognostic viewpoints. Putaminal NAA/Cr reduction was significant in MSA-P patients compared with PD and control subjects, as previously reported.[11–14] However, as discussed above, the putaminal volume effect could influence the significance of putaminal NAA/Cr reduction, particularly in patients with advanced disease. Although brainstem and cerebellar involvement is an important and specific finding in differentiating MSA-P from PD,[25 32] the sensitivity of both clinical and MRI evaluations of these abnormalities is relatively low.[7 26] Based on our results, we believe that ^{1}H-MRS assessment of the pontine base would be of considerable value in the differential diagnosis between MSA-P and PD. However, combined ^{1}H-MRS study of the pontine base and putamen can provide a more sensitive differentiation between MSA-P and PD than a conventional single regional study, such as that of the putamen.

The cerebral hemisphere is involved more extensively in MSA than previously believed. Recently, Abe *et al* reported a significant decrease in NAA/Cr in MSA, involving Brodmann's areas 6, 8, and 46.[14] Moreover, Spargo *et al*

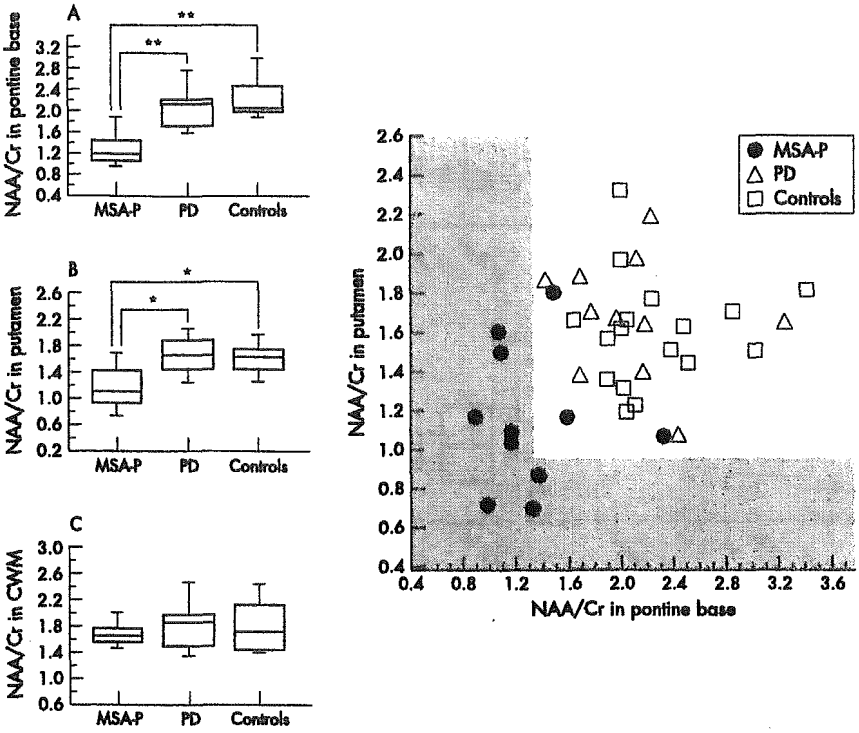

Figure 6 Box and whisker plot of the NAA/Cr ratio in the pontine base (A), putamen (B) and cerebral white matter (CWM, C) compared between MSA-P, PD, and controls. D is a scatter plot of the individual NAA/Cr data in the pontine base *v* putamen including MSA-P, PD, and control subjects. The scaled area corresponds to the mean−2 SD of NAA/Cr in the pontine base and putamen of control subjects. *p=0.002, **p<0.0001 by Scheffé's test, respectively. NAA, N-acetylaspartate; Cr, creatine; MSA-P, multiple system atrophy with parkinsonism predominant.

reported 18.7% and 21.4% neuronal loss in the primary and supplementary motor cortex, respectively.[33] In addition, the degree of atrophy in cerebral hemispheric areas varies between individuals, often becoming severe in long standing cases.[34] We found a mild overall reduction of NAA/Cr in CWM with a more significant NAA/Cr reduction in the subgroup with a longer duration of illness. This finding is in good agreement with previous ^{1}H-MRS reports and pathological observations.

Davie *et al*[11] reported a significant reduction of Cho/Cr ratio suggesting reduced membrane turnover in the lentiform nucleus in MSA, perhaps as result of cell loss. In the present study, Cho/Cr showed little change throughout the course of disease in the putamen, pontine base, and CWM, in agreement with other reports.[12–14 16] The relevance of this discrepancy is uncertain. One possible explanation is the difference of technical factors such as size of VOI and echo time. On the other hand, pathological study shows not only cell loss but also widely and variously distributed myelin degeneration in MSA brains that may increase the Cho.[35] Thus, heterogeneity of lesions in association with disease stage also may influence the Cho/Cr result. Further longitudinal studies and comparison of ^{1}H-MRS with histological findings will be needed to clarify the uncertainty as to the Cho/Cr ratio in MSA.

In conclusion, localised ^{1}H-MRS at 3.0 T in multiple regions showed widespread neuronal and axonal involvement in patients with MSA. NAA/Cr reduction in the pontine base provided a significant diagnostic marker for MSA irrespective of the disease form of MSA-P or MSA-C, disease duration, symptomatic manifestations, or MRI abnormalities. Moreover, combined ^{1}H-MRS study of the pontine base and putamen proved particularly effective in differentiating MSA from PD. We believe that ^{1}H-MRS would provide an early and accurate MSA diagnosis, an enhanced understanding of its pathogenetic mechanism, and the conclusiveness needed for future therapeutic trials.

Authors' affiliations
H Watanabe, M Katsuno, M Sugiura, K Hamada, Y Okada, M Hirayama, G Sobue, Department of Neurology, Nagoya University Graduate School of Medicine, Japan
H Fukatsu, T Ishigaki, Department of Radiology, Nagoya University Graduate School of Medicine, Japan

Competing interest: none declared

REFERENCES

1 **Graham JG,** Oppenheimer DR. Orthostatic hypotension and nicotine sensitivity in a case of multiple system atrophy. *J Neurol Neurosurg Psychiatry* 1969;32:28–34.
2 **Quinn N.** Multiple system atrophy–the nature of the beast. *J Neurol Neurosurg Psychiatry* 1989;52:78–89.
3 **Gilman S,** Low PA, Quinn N, *et al.* Consensus statement on the diagnosis of multiple system atrophy. *J Neurol Sci* 1999;163:94–8.
4 **Sobue G,** Terao S, Kachi T, *et al.* Somatic motor efferents in multiple system atrophy with autonomic failure: a clinico-pathological study. *J Neurol Sci* 1992;112:113–25.
5 **Wenning GK,** Ben-Shlomo Y, Magalhes M, *et al.* Clinicopathological study of 35 cases of multiple system atrophy. *J Neurol Neurosurg Psychiatry* 1995;58:160–6.
6 **Lantos P.** The definition of multiple system atrophy: A review of recent developments. *J Neuropathol Exp Neurol* 1998;57:1099–111.
7 **Watanabe H,** Saito Y, Terao S, *et al.* Progression and prognosis in multiple system atrophy; an analysis of 230 Japanese patients. *Brain* 2002;125:1070–83.
8 **Ross B,** Michaelis T. Clinical applications of magnetic resonance spectroscopy. *Magn Reson Q* 1994;10:191–247.
9 **Davie CA.** The role of spectroscopy in parkinsonism. *Mov Disord* 1998;13:2–4.
10 **Rudkin TM,** Arnold DL. Proton magnetic spectroscopy for the diagnosis and management of cerebral disorders. *Arch Neurol* 1999;56:919–26.
11 **Davie CA,** Wenning GK, Barker GJ, *et al.* Differentiation of multiple system atrophy from idiopathic Parkinson's disease using proton magnetic resonance spectroscopy. *Ann Neurol* 1995;37:204–10.
12 **Federico F,** Simone IL, Lucivero V, *et al.* Proton magnetic resonance spectroscopy in Parkinson's disease and atypical parkinsonian disorders. *Mov Disord* 1997;12:903–9.
13 **Federico F,** Simone IL, Lucivero V, *et al.* Usefulness of proton magnetic resonance spectroscopy in differentiating parkinsonian syndromes. *Ital J Neurol Sci* 1999;20:223–9.
14 **Abe K,** Terakawa H, Takanashi M, *et al.* Proton magnetic resonance spectroscopy of patients with parkinsonism. *Brain Res Bull* 2000;52:589–95.

15 **Terakawa H**, Abe K, Watanabe Y, *et al.* Proton magnetic resonance spectroscopy (1H MRS) in patients with sporadic cerebellar degeneration. *J Neuroimaging* 1999;9:72–7.
16 **Clarke CE**, Lowry M. Basal ganglia metabolite concentrations in idiopathic Parkinson's disease and multiple system atrophy measured by proton magnetic resonance spectroscopy. *Eur J Neurol* 2000;7:661–5.
17 **Hu MTM**, Simmons A, Glover A, *et al.* Proton magnetic resonance spectroscopy of the putamen in Parkinson's disease and multiple system atrophy. *Mov Disord* 1998;13:182.
18 **Clarke CE**, Lowry M. Systematic review of proton magnetic resonance spectroscopy of the striatum in parkinsonian syndromes. *Eur J Neurol* 2001;8:573–7.
19 **Bomsdorf H**, Helzel T, Kunz D, *et al.* Spectroscopy and imaging with a 4 Tesla whole-body MR system. *NMR Biomed* 1988;1:151–8.
20 **Hetherington HP**, Pan JW, Chu W-J, *et al.* Biological and clinical MRS at ultra-high field. *NMR Biomed* 1988;10:360–71.
21 **Gruetter R**, Weisdorf SA, Rajanayagan V, *et al.* Resolution improvements in vivo NMR spectra with increased magnetic field strength. *J Magn Reson* 1988;135:260–4.
22 **Caine DB**, Snow BJ, Lee C. Criteria for diagnosing Parkinson's disease. *Ann Neurol* 1992;32:S125–7.
23 **Savoiardo M**, Strada L, Girotti F, *et al.* Olivopontocerebellar atrophy: MR diagnosis and relationship to multiple system atrophy. *Radiology* 1990;174:693–6.
24 **Kraft E**, Schwarz J, Trenkwalder C, *et al.* The combination of hypointense and hyperintense signal changes on T2-weighted magnetic resonance imaging sequences: a specific marker of multiple system atrophy? *Arch Neurol* 1999;56:225–8.
25 **Konagaya M**, Sakai M, Matsuoka Y, *et al.* Pathological correlate of the slitlike changes on MRI at the putaminal margin in multiple system atrophy. *J Neurol* 1999;246:142–3.
26 **Schrag A**, Good CD, Miszkiel K, *et al.* Differentiation of atypical parkinsonian syndromes with routine MRI. *Neurology* 2000;54:697–02.
27 **Moffett JR**, Namboodiri MAA, Cangro CB, *et al.* Immunohistochemical localization of N-acetylaspartate in rat brain. *Neuroreport* 1991;2:131–4.
28 **Simmons ML**, Frondoza CG, Coyle JT. Immunohistochemical localization of N-acetylaspartate with monoclonal antibodies. *Neuroscience* 1991;45:37–45.
29 **Urenjak J**, Williams SR, Gadian DG, *et al.* Specific expression of N-acetylaspartate in neurons, oligodendrocyte type-2 astrocyte progenitors, and immature oligodendrocyte in vitro. *J Neurochem* 1992;59:55–61.
30 **Bhakoo KK**, Pearce D. In vivo expression of N-acetylaspartate by oligodendrocytes: implications for proton magnetic resonance spectroscopy signal in vivo. *J Neurochem* 2000;74:254–62.
31 **Bjartmar C**, Battistuta J, Terada N, *et al.* N-acetylaspartate is an axon-specific marker of mature white matter in vivo: a biochemical and immunohistochemical study on the rat optic nerve. *Ann Neurol* 2002;51:51–8.
32 **Litvan I**, Goetz CG, Jankovic J, *et al.* What is accuracy of the clinical diagnosis of multiple system atrophy? *Arch Neurol* 1997;54:937–44.
33 **Spargo E**, Papp MI, Lantos PL. Decrease in neuronal density in the cerebral cortex in multiple system atrophy. *Eur J Neurol* 1996;3:450–6.
34 **Konagaya M**, Sakai M, Matsuoka Y, *et al.* Multiple system atrophy with remarkable frontal lobe atrophy. *Acta Neuropathol (Berl)* 1999;97:423–8.
35 **Matsuo A**, Akiguchi I, Lee GC, *et al.* Myelin degeneration in multiple system atrophy detected by unique antibodies. *Am J Pathol* 1998;153:671–6.

DOI: 10.1093/brain/awh020 Advanced Access publication November 7, 2003 *Brain* (2004), 127, 203–211

Nerve excitability properties in Charcot–Marie–Tooth disease type 1A

Hiroyuki Nodera,[1] Hugh Bostock,[4] Satoshi Kuwabara,[2] Takashi Sakamoto,[1] Kotaro Asanuma,[1] Sung Jia-Ying,[2] Kazue Ogawara,[2] Naoki Hattori,[3] Masaaki Hirayama,[3] Gen Sobue[3] and Ryuji Kaji[1]

[1]*Department of Clinical Neuroscience, Graduate School of Medicine, University of Tokushima, Tokushima,* [2]*Department of Neurology, Chiba University, Chiba,* [3]*Department of Neurology, Nagoya University, Nagoya, Japan and* [4]*Sobell Department of Neurophysiology, Institute of Neurology, Queen Square, London, UK*

Correspondence to: Ryuji Kaji, MD, PhD, Department of Clinical Neuroscience, University of Tokushima, 2-50-1 Kuramotocho, Tokushima City, 770-8503 Japan E-mail: rkaji@clin.med.tokushima-u.ac.jp

Summary

Charcot–Marie–Tooth disease type 1A (CMT1A) is commonly considered a prototype of a hereditary demyelinating polyneuropathy. Apart from the myelin involvement, there has been little information on axonal membrane properties in this condition. Taking advantage of the uniform nature of the disease process, we undertook the *in vivo* assessment of multiple axonal excitability properties at the median nerve in nine CMT1A patients with *PMP22* (peripheral myelin protein 22) gene duplication and 53 controls. The thresholds of CMT1A patients were much higher than normal, and threshold electrotonus (TE) exhibited a consistent pattern of abnormalities: early steep changes (fanning out) of both hyperpolarizing and depolarizing responses were followed by increased inward rectification to hyperpolarizing currents and unusually fast accommodation to depolarizing currents. Strength–duration time constants and the shapes of recovery cycles were normal, although refractoriness and superexcitability were reduced relative to controls. The high thresholds and early fanning out of electrotonus indicated altered cable properties, such that a greater proportion than normal of applied currents reached internodal rather than nodal axolemma. The rapid accommodation to depolarizing currents suggested activation of fast K^+ channels, which are normally sequestered from the nodal membrane. The excitability abnormalities are therefore consistent with a demyelinating pathology and exposure or spread of K^+ channels from under the myelin. It remains to be seen whether the TE abnormalities in CMT1A, which resemble previous recordings from normal immature rats, can be distinguished from those in acquired demyelinating neuropathies.

Keywords: Charcot–Marie–Tooth disease type 1A; paranode; membrane properties; threshold tracking; potassium channel

Abbreviations: CIDP = chronic inflammatory demyelinating polyneuropathy; CMAP = compound muscle action potential; CMT1A = Charcot–Marie–Tooth disease type 1A; CV = conduction velocity; DL = distal motor latency; PMP22 = peripheral myelin protein 22; SNAP = sensory nerve action potential; TE = threshold electrotonus

Introduction

Charcot–Marie–Tooth disease type 1A (CMT1A) is the most common form of hereditary motor and sensory neuropathy and its hallmark is diffuse demyelination (Dyck *et al.*, 1993; Birouk *et al.*, 1997). However, secondary axonal degeneration is common and its degree determines the patient's functional disability (Hattori *et al.*, 2003; Krajewski *et al.*, 2000; Hanemann and Gabreels-Festen, 2002). To date, the pathophysiology of the secondary axonal degeneration in CMT1 is unknown, although abnormal axon–Schwann cell interaction has been considered to play a major role (Sahenk and Mendell, 1999*a*; Kamholz *et al.*, 2000; Maier *et al.*, 2002). Intact Schwann cells are important in maintaining axonal integrity and development (Peles and Salzer, 2000; Martini, 2001; Scherer and Arroyo, 2002), so it would be reasonable to assume that in CMT1A abnormalities exist in axonal membrane properties, as well as in myelin.

Measurements of axonal excitability properties by threshold tracking have recently shed light on a variety of conditions affecting peripheral nerves (Bostock *et al.*, 1998; Burke *et al.*, 2001). The excitability properties are particularly sensitive to membrane potential, but also depend on nodal and internodal ion channels, as well as the passive

membrane properties, such a nodal width, and the extent to which the internodal axonal compartment is electrically isolated from the nodal compartment (Bostock *et al.*, 1998). Although many of these parameters are expected to be altered in demyelinating disease, several clinical studies have failed to reveal a clear-cut pattern of excitability changes related to demyelination. Thus a study of chronic inflammatory demyelinating polyneuropathy (CIDP) found raised thresholds but a shorter strength–duration time constant and no consistent changes in threshold electrotonus (Cappelen-Smith *et al.*, 2001). Studies of multifocal motor neuropathy have found evidence of membrane hyperpolarization distal to sites of conduction block (Kiernan *et al.*, 2002*b*), reduced Na^+ conductance (Priori *et al.*, 2002) and normal membrane properties proximal to sites of block (Cappelen-Smith *et al.*, 2002), but at the sites of conduction block, where demyelination has been reported (Kaji *et al.*, 1993), thresholds are very high and specific excitability changes relatable to demyelination have not been reported. A study of axonal and demyelinating forms of Guillain–Barré syndrome (Kuwabara *et al.*, 2002*a*) also failed to find any changes in nerve excitability properties at the wrist that could be directly related to the demyelination, probably because the major pathology occurred more distally in these patients. It has previously been argued that the reason why threshold electrotonus studies have failed to reveal consistent abnormalities in demyelinating neuropathies is because axons and nodes are affected non-uniformly, and fibres demyelinated at the point of stimulation will preferentially be excited at adjacent normal nodes, or other, more normal fibres will be excited in their place (Bostock *et al.*, 1998). This argument should be less applicable to CMT1A, in which it is possible to limit cases to a well-defined genetic defect [duplication of the *PMP22* (peripheral myelin protein 22) gene] and axons are affected relatively uniformly.

This study was therefore undertaken to test the hypothesis that CMT1A patients, unlike those with previously studied acquired demyelinating diseases, would exhibit a consistent pattern of abnormal excitability measures. A further aim was to test for secondary changes in axonal membrane properties, such as changes in membrane potential, which could not be related directly to altered myelination but which might be related to the secondary axonal degeneration. In the event, a consistent pattern of abnormal nerve excitability properties was found, which was consistent with demyelination, but there was little evidence of degeneration, or excitability changes that might be related to degeneration, in the sample of patients studied.

Patients and methods

Patients

Recordings were made from nine patients with genetically proven CMT1A (aged 11–75 years; mean 48.1 years; seven males and two females) from three university hospitals in Japan. All patients showed typical but variable clinical features of CMT type 1, such as diffuse areflexia/hyporeflexia, length-dependent sensory loss, distal atrophy and foot deformities. A fluorescence *in situ* hybridization-based assay identified the 1.5 Mb duplication on chromosome 17p11.2–12 containing the *PMP22* gene in all the subjects. No patient had a past history of diabetes, connective tissue disease, malignancy, electrolyte abnormality or use of neurotoxic drugs or steroids. All the patients had a clear family history of similar symptoms and signs of autosomal dominant inheritance. All the patients (and a parent for a minor) gave informed consent to participation in the study. This study was performed in accordance with the principles embodied in the Declaration of Helsinki and the protocol was approved by institutional review boards of all participating hospitals.

Conventional nerve conduction studies

Nerve conduction studies were performed with percutaneous stimulating and recording electrodes. The distal motor latency (DL), motor nerve conduction velocity (CV) and compound muscle action potentials (CMAP) were elicited with distal and proximal stimulation from the median (in the wrist with 7 cm stimulating–recording distance, and in the elbow), ulnar (in the wrist with 7 cm stimulating–recording distance; and in the forearm) and tibial (in the ankle with 8 cm stimulating–recording distance, and in the knee) nerves. Sensory nerve action potentials (SNAPs) were recorded antidromically from the median, ulnar and sural nerves using surface recording electrodes and stimulating–recording distances of 13, 11 and 14 cm respectively.

Nerve excitability measures

Studies were performed using a recently described protocol (Kiernan *et al.*, 2000) designed to measure multiple nerve excitability parameters rapidly.

CMAPs were recorded from thenar muscles using surface electrodes over the abductor pollicis brevis on the dominant hand side, with the active electrode at the motor point and the reference on the proximal phalanx. The EMG signal was amplified (gain 1000, bandwidth 1.6 Hz to 2 kHz) and digitized by a computer (486PC) with an A/D board (DT2812; Data Translation, Marlboro, MA, USA) using a sampling rate of 10 kHz. Stimulus waveforms generated by the computer were converted to current with a purpose-built isolated linear bipolar constant-current stimulator (maximum output ± 100 mA). The stimulus currents were applied via non-polarizable electrodes (Unique Medical, Tokyo, Japan), with the active electrode over the median nerve at the wrist and the reference electrode 10 cm proximal over muscle. Stimulation and recording were controlled by QTRAC software (©Institute of Neurology, London, with multiple excitability protocol TRONDXM).

Test current pulses of 0.2 or 1 ms were applied at 0.8 s intervals, and were combined with suprathreshold condition-

Table 1 *Results of the nerve conduction studies*

Nerve	DL (ms)	CMAP amplitude (mV)	Motor CV (m/s)	SNAP amplitude (μV)	Sensory CV (m/s)
Median	8.5 (6.9–10.2)	4.7 (1.8–8.9)	22.3 (16–39)	2.1 (0–6.8)	22.4 (18–28; $n^* = 5$)
Ulnar	7.4 (5.9–9.1)	3.1 (0.9–4.2)	22.2 (15–38)	0.5 (0–3.0)	23 (20–26; $n = 2$)
Tibial	10.3 (6.5–12.1)	1.2 (0–3.2)	18.7 (13–35)		
Sural				1.47 (0–12)	23 (16–29; $n = 2$)

Data are mean (range). There were nine patients (seven men, two women), with mean age 48.1 years (range 11–75 years). n^* is the number of patients in whom CV was obtainable (i.e. presence of SNAP). DL = distal latency; CMAP = compound muscle action potential; CV = conduction velocity; SNAP = sensory nerve action potential.

ing stimuli or subthreshold polarizing currents as required. The polarizing, conditioning and test current pulses were all delivered through the same electrodes. The amplitude of the CMAP was measured from baseline to negative peak. For all tracking studies, the target CMAP was set to 40% of maximum. Skin temperature was recorded using an adhesive probe over the nerve, adjacent to the stimulation electrode, to monitor temperature close to the site where axonal excitability was tested. The sequence of recordings followed that previously described (Kiernan *et al.*, 2000). Stimulus–response curves were recorded separately for test stimuli of durations 0.2 and 1 ms. The stimuli were increased in 6% steps, with two responses averaged for each step, until three averages were considered maximal. The ratio between the 0.2 and 1 ms stimuli required to evoke the same response was used to estimate the strength–duration time constant of axons of different threshold. A target response was then set at 40% of the maximum and the 1.0 ms test stimuli adjusted automatically by the computer to maintain this peak CMAP amplitude. Proportional tracking was used, whereby the change in stimulus amplitude from one trial to the next was made proportional to the 'error', or the difference between the last response and the target response (Bostock *et al.*, 1998). The slope of the stimulus–response curve was used to set the constant of proportionality and to optimize the tracking efficiency. Prolonged subthreshold currents were used to alter the potential difference across the internodal as well as the nodal axonal membrane. The changes in threshold associated with these electrotonic changes in membrane potential normally have a similar time course and are known as threshold electrotonus (TE) (Bostock *et al.*, 1998). Threshold tracking was used to record the changes in threshold induced by 100 ms polarizing currents, set to 40% (depolarizing) and −40% (hyperpolarizing) of the control threshold current. Three stimulus combinations were tested in turn: (i) test stimulus alone (to measure the control threshold current); (ii) test stimulus + depolarizing conditioning current; and (iii) test stimulus + hyperpolarizing conditioning current. Threshold was tested at 26 time points (maximum separation 10 ms) before, during and after the 100 ms conditioning currents. Each stimulus combination was repeated until three valid threshold estimates were recorded, as judged by the response being within 15% of the target response or alternate responses being either side of the target. We checked for the lack of CMAP response in all the raw traces after applying only conditioning stimulation.

The current–threshold relationship was tested with 1 ms pulses at the end of 200 ms polarizing currents, which were altered in 10% steps from +50% (depolarizing) to −100% (hyperpolarizing) of the control threshold. As with the conventional TE protocol, stimuli with conditioning currents were alternated with test stimuli alone, and each stimulus combination was repeated until three valid threshold estimates had been obtained.

The final part of the protocol recorded the recovery of excitability following a supramaximal conditioning stimulus. These changes were recorded at 18 conditioning ($1/n$) test intervals, decreasing from 200 to 2 ms in approximately geometrical progression. Three stimulus combinations were tested in turn: (i) unconditioned test stimulus (of 1 ms duration) tracking the control threshold; (ii) supramaximal conditioning stimulus (1 ms duration) alone; and (iii) conditioning + test stimuli. The response to (ii) was subtracted on-line from the response to (iii) before the test CMAP was measured, so that the conditioning maximal CMAP did not contaminate the measured response when the conditioning–test interval was short. Each stimulus combination was repeated until four valid threshold estimates had been obtained.

Control data

For threshold tracking studies, control data were obtained from 53 healthy individuals with mean age 43.1 years (range 23–84 years) at Chiba University Hospital. Given the fact that additional control data from an 8-year-old girl (not included for analysis at the parent's request) has shown a similar trend of the nerve excitability properties to the adult controls, data from an 11-year-old CMT1A patient was included for the study. All subjects (and a parent for a minor) gave informed consent.

Data analysis

Values for the excitability measures obtained in the present study were compared with normative data. The Mann–Whitney *U* test or repeated measures ANOVA (analysis of variance) was used for comparison using SPSS 11.0J (Tokyo, Japan). TEd (5 ms), TEd (10–20 ms) and TEd (90–100 ms) were the mean threshold reductions at or between the specific

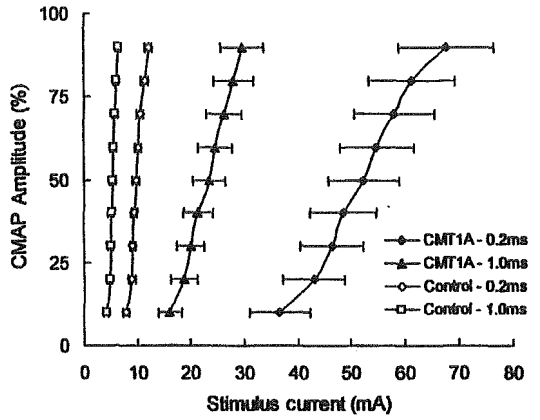

Fig. 1 Absolute stimulus–response curves (mean ± SEM) of median motor axons at the wrist in 53 healthy controls and nine CMT1A patients for two stimulus durations (0.2 and 1.0 ms). The threshold currents were significantly higher and the slopes of the curves were reduced, with greater variability of thresholds, in the patient group.

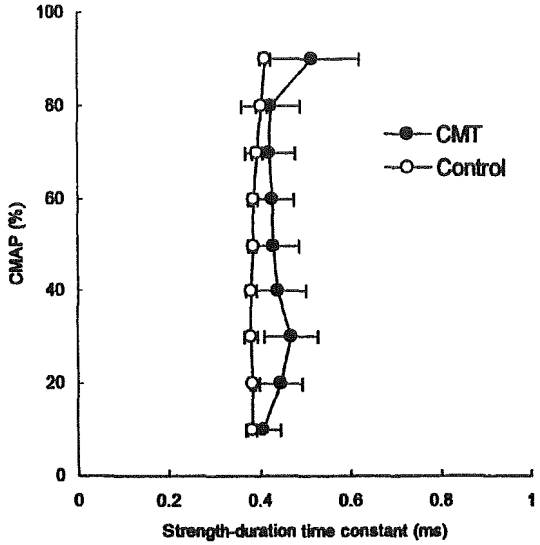

Fig. 2 The strength–duration time constant in CMT1A patients and controls (mean ± SEM). Although the strength–duration time constant was slightly longer in CMT1A than in controls, no significant change was demonstrated.

latencies after the onset of depolarizing current, and TEh (10–20 ms), TEh (20–40 ms) and TEh (90–100 ms) were the corresponding threshold changes after the onset of hyperpolarizing current. TEd (16 ms) – TEd (5 ms) was the difference in the threshold reductions at the respective latencies.

Results

Clinical features and nerve conduction study

Clinical profiles of the patients are shown in Table 1. Electrophysiological features showed diffuse demyelinative sensorimotor polyneuropathy with uniform conduction slowing, typical of CMT1, in all the subjects (Birouk *et al.*, 1997). Note that the median CMAP amplitudes were normal in 66% of the patients. As expected, there was an inverse relationship between age and median CMAP amplitude ($r = -0.61$, $y = -0.0637x + 7.9344$), but otherwise no age effect was observed in the analyses described below.

It has been shown that serum potassium level significantly affects axonal excitability (Kiernan *et al.*, 2002*a*; Kuwabara *et al.*, 2002*b*); the level was obtained in six of the nine subjects and all values were within normal limits (mean 4.1 mEq/l, range 3.7–5.3 mEq/l, normal, 3.5–5.5 mEq/l). As there was no significant change in the parameters assessed below between those from all the CMT patients and from patients with normal serum potassium levels, the remaining statistical analyses compared all the CMT patients with the controls.

Multiple excitability measures using threshold tracking

Stimulus–response curves

In the stimulus–response curves, the threshold currents in the nine CMT1A patients were significantly higher than those in the 53 healthy controls (Fig. 1). The stimulation current required to produce a minimal (10%) CMAP in the CMT1A patients was more than three times as high as that required to produce a maximal CMAP in healthy controls (Fig. 1). To produce a CMAP 40% of maximum, the mean absolute current for the 0.2 ms test stimulus was 48.7 ± 18.8 mA in the CMT1A patients and 9.5 ± 0.6 mA in the controls ($P < 0.001$). The mean absolute current for the 1.0 ms test stimulus was 21.5 ± 8.2 mA in the patients and 5.3 ± 0.5 mA in the controls ($P < 0.001$). Despite the significantly greater stimulation current in the patients, the test was well tolerated by the patients, possibly because of impaired sensation.

Strength–duration properties

Although the strength–duration time constant was slightly increased in the CMT group, there was no significant difference between the two groups (Fig. 2). The strength–duration time constant was fairly stable in both controls and CMT1A patients throughout the different CMAP amplitude levels. However, in CMT1A patients, an inverse relationship between the maximum CMAP amplitude and the strength–duration time constant at the 50% maximum CMAP level ($r = -0.51$) was found.

Recovery cycle

The patterns of the recovery cycles were similar in controls and CMT patients, the relative refractory period lasting <3 ms, supernormality being maximal at the 5-ms conditioning–test interval and late subnormality maximal at ~40 ms (Fig. 3). The extent of the changes in threshold during the refractory period was significantly greater in the control group at the 2-

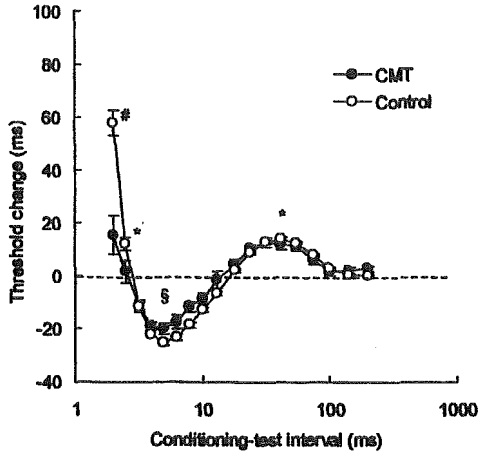

Fig. 3 The recovery cycle in CMT1A patients and controls (mean ± SEM). Nerves from patients with CMT1A showed less pronounced threshold changes in relative refractory and supernormal periods than controls, though durations of each period were similar. $P < 0.0007$; §$P < 0.02$; *not significant.

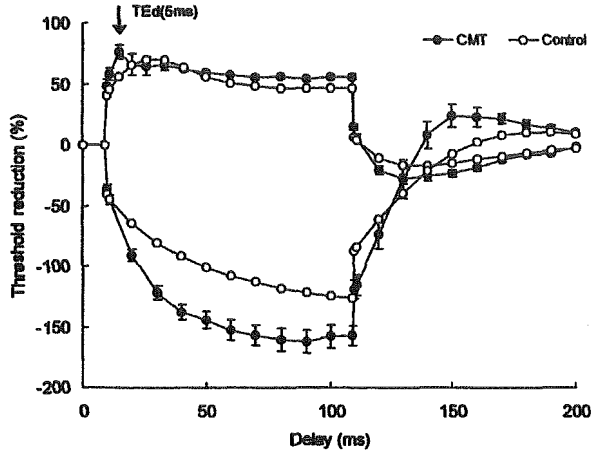

Fig. 4 Threshold electrotonus (mean ± SEM). In CMT1A patients, accommodation to depolarizing currents was stronger and occurred earlier than in controls. There was generalized widening out of the curves in CMT1A (fanning out) and greater accommodation to long hyperpolarizing currents.

ms conditioning–test interval ($P < 0.0007$), but not significantly different at the 2.5-ms interval ($P = 0.10$). For supernormality, the control group demonstrated a greater threshold change than the CMT group ($P < 0.02$), but there was no difference in late subnormality ($P = 0.88$) (Fig. 3). These findings of normal durations of the periods and reduced threshold changes in the patient group compared with those in controls are similar to the data in chronic inflammatory demyelinating polyneuropathy (Cappelen-Smith *et al.*, 2001).

Threshold electrotonus and current–voltage relationships

The most striking abnormalities in excitability parameters were revealed by the recordings of TE (Fig. 4). Table 2 documents comparisons of various excitability measures. Significant changes were observed in the responses to hyperpolarizing current. These were most pronounced in the early part of the responses [TEh (10–20 ms) and TEh (20–40 ms)] (Table 2) but still present at 90–100 ms. A closer look at the early part of the response to depolarizing current [TEd (10–20ms)] also disclosed steeper than normal changes. Because families of these electrotonus response curves can resemble the ribs of a Japanese fan, coming from a point near the origin of the plot (Fig. 6B), these changes can be described as a 'fanning-out' of the responses (Kaji, 1997). The more pronounced curvature in the CMT hyperpolarizing electrotonus suggests more accommodation due to activation of inward rectification by the hyperpolarization-activated current I_H (see Discussion).

The depolarizing electrotonus was more complicated, the CMT patients exhibiting first more, then less, and then more threshold reduction than the controls. At 5 ms, the depolarizing current induced a significantly greater threshold reduction than in controls (fanning-out). This was, however, quickly followed by an accommodative fall in threshold, between 5 and 16 ms. At longer delays, the CMT patients again showed a significantly greater threshold reduction than controls.

The current–threshold relationship (Fig. 5) also showed evidence of contrasting changes in passive and voltage-dependent membrane properties. With small currents, the slope of the current–threshold relationship was reduced, which, like the early fanning out of the TE, indicates that a greater fraction of the applied current was reaching the internodal axon (see Discussion). With larger currents, however, the slope was increased, in both the depolarizing and hyperpolarizing directions, until the absolute threshold changes returned towards and crossed the control curves respectively, indicating increased outward and inward rectification. Neither the TE nor the current–threshold relationship revealed correlation between CMAP amplitude and the extent of the nerve excitability abnormalities.

Discussion

The present study has shown that, in CMT1A, recognized as a polyneuropathy with uniform demyelination, there are consistent changes in nerve excitability properties, especially in resting thresholds and in TE. These changes were unlikely to be related to axonal degeneration, as CMAP amplitudes were fairly well preserved in the tested nerves, and there was no correlation between CMAP amplitude and the extent of the electrotonus abnormalities. Here we will consider the likely biophysical basis of the excitability changes observed.

Table 2 *Comparison of various excitability measures in TE*

	CMT1A (mean ± SD)	Control (mean ± SD)	*P*
TEd (10–20 ms)	65.5 ± 17.0	68.6 ± 4.9	0.73
TEd (90–100 ms)	56.1 ± 6.0	46.9 ± 4.8	< 0.001
TEh (10–20 ms)	−106.4 ± 15.2	−72.5 ± 6.5	< 0.001
TEh (20–40 ms)	−133.0 ± 16.3	−91.0 ± 10.6	< 0.001
TEh (90–100 ms)	−157.1 ± 25.7	−125.3 ± 24.1	< 0.004
TEd (5 ms)	76.2 ± 16.7	56.2 ± 3.7	< 0.001
TEd (16 ms) – TEd (5 ms)	−11.5 ± 23.9	14.0 ± 3.2	< 0.001

Values are threshold reduction (%).

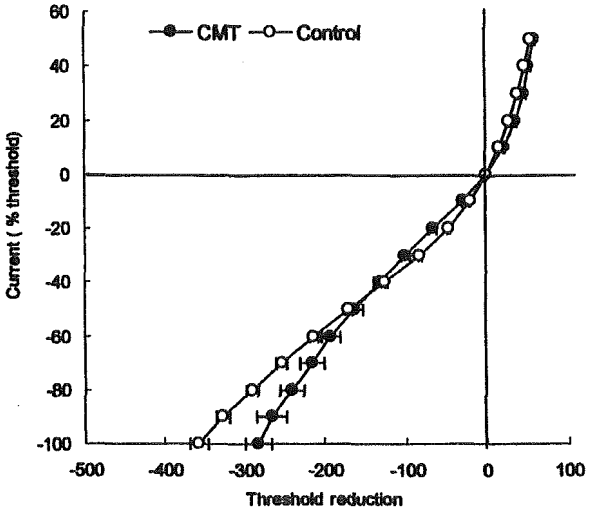

Fig. 5 The current–threshold relationship (mean ± SEM) demonstrated no statistical difference between the CMT1A and controls. However, the CMT group had a tendency to have greater threshold changes to depolarizing and weak hyperpolarizing currents consistent with fanning out in TE, and smaller changes in response to strong hyperpolarizing currents.

Increased resting threshold and early fanning out of threshold electrotonus

Figure 6 shows a simplified equivalent circuit for a segment of axon (node + internode), which accounts for the fast and slow phases of electrotonus and threshold (Barrett and Barrett, 1982; Yang *et al.*, 2000). It shows how an applied current (I) is divided into two components, a nodal component (I_n), which alters the potential on the nodal membrane by an amount I_nR_n (Ohm's law), and an internodal component (I_i), which initially changes the potential on the internodal axolemma at the rate I_i/C_i (as $C_i = I_i * t$). The initial proportion of current that crosses the nodal membrane (I_n/I) is set by the resistance ratio $R_{il}/(R_{il} + R_n)$, whereas the proportion crossing the internodal membrane (I_i/I) is $R_n/(R_{il} + R_n)$. The substantial increase in resting threshold current, and the increase in the early fanning out of TE indicate that in CMT1A the proportion of applied current crossing the nodal membrane is decreased and the proportion crossing the internodal membrane is correspondingly increased, i.e. that R_{il} is reduced in relation to R_n. If R_n were increased, the current threshold would fall, so we conclude that there is a reduction in R_{il}, which could be caused either by thin or 'leaky' myelin, or by a loosening of the axon–Schwann cell paranodal seal; both of these changes are consistent with the pathology of CMT1A. The reduction in R_{il} reduces I_n/I, so that the applied current has to be increased to reach the same threshold depolarization of the node. The reduction in R_{il} also increases I_i/I and the initial rate of polarization of the internodal axolemma. In a previous paper we introduced the idea of the 'fan' origin of TE (Bostock 1995; Kaji 1997; Yang *et al.*, 2000): the point (found by projecting back the tangents to the initial portion of slow electrotonus to the resting threshold) from which the slow electrotonus appears to originate (O in Fig. 6B). The time interval (t_f) from the fan origin to the time of current application was shown to be $C_iR_{il}(R_{il} + R_n)/R_n$, for the simplified circuit of Fig. 6A. A reduction in R_{il} reduces t_f and causes a more acute fanning-out of electrotonus.

Increased inward rectification in CMT1A

On the hyperpolarizing side, the early increased fanning out of TE in CMT1A is not maintained (Yang *et al.*, 2001). Inward rectification, most likely due to the slowly activating hyperpolarization-activated current I_H, sets in, so that by 100 ms the CMT1A and control curves are approaching each other, and by 200 ms (the time used for the current–threshold measurements in Fig. 5) the curves cross over for hyperpolarizing currents in excess of 40% of threshold. Greater activation of I_H during hyperpolarization TE in CMT1A patients is also indicated by the excitability overshoot after the end of the hyperpolarizing current at 150 ms, since I_H deactivates slowly. Although the TE and current–threshold data thus both indicate increased activation of I_H in CMT1A patients relative to normal controls, it is not clear whether this implies any alteration in axonal channel function (e.g. channel density). Because threshold currents are abnormally high in CMT1A, the polarizing currents used in the TE and current–threshold recordings are also abnormally high, so that the degree of hyperpolarization of the internodal axon must be much greater. It is therefore quite possible that the increased activation of I_H in CMT1A patients simply reflects

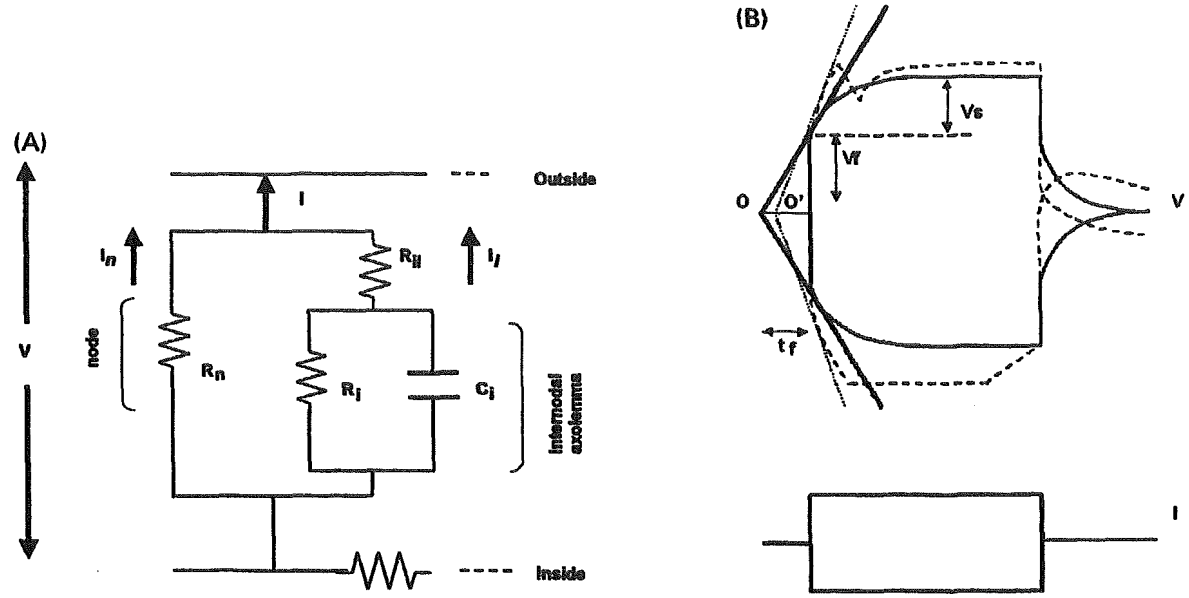

Fig. 6 A mathematical model of TE based solely on passive membrane properties. (**A**) A simplified equivalent circuit of myelinated axon (passive components only) (Barrett and Barrett, 1982), which generates fast and slow components of electrotonus. R_n, nodal resistance; R_{II}, internodal leakage resistance (access resistance to internodal axolemma, through and under the myelin sheath); R_i and C_i, resistance and capacitance of internodal axon. (**B**) Electrotonic changes in membrane potential (V) to long current pulses (I) predicted by the circuit in (**A**) in controls (solid lines) and CMT1A (dashed lines). V_f and V_s, fast and slow components of electrotonus; O and O′, apparent origins of fanning determined by lines tangential to the initial parts of the slow component; t_f, the time from O and O′ to the start of the current pulses. Note that the t_f is shorter in CMT1A than that in controls.

this increased membrane hyperpolarization rather than any abnormality in ion channels.

Rapid outward rectification in CMT1A

On the depolarizing side, the early increased fanning out of TE in CMT1A is much shorter-lived and quickly gives way to rapid accommodation. This rapid accommodation is similar to that previously seen in young rats, which was shown to be due to activation of fast K^+ channel channels that were blocked by 4-aminopyridine (Yang *et al.*, 2000). Whereas in normal, mature myelinated axons the fast K^+ channel channels $K_v1.1$ and $K_v1.2$ are concentrated in the juxtaparanodal region of the internode (Vabnick *et al.*, 1999; Girault and Peles, 2002), where they only affect slow components of electrotonus, in CMT1A they are activated rapidly by applied currents, either because they have spread to the nodal region, or because disruption of the axon–Schwann cell paranodal seal allows more current to reach the juxtaparanodal zone. Prior observations in the experimental demyelination demonstrated similar participation of the internodal K^+ channel channels to action potentials, in accordance with the present findings (Bostock *et al.*, 1981; Brismar, 1981; Chiu and Ritchie, 1981). An alternative viewpoint, suggested by the resemblance of TE in CMT1A patients to that in immature rats (Yang *et al.*, 2000), is that overproduction of the myelin protein PMP22 in the disease may inhibit normal nodal maturation. This interpretation is in accordance with studies demonstrating that axonal cytoskeleton in CMT1A is similar to those in immature axons (Sahenk *et al.*, 1999*b*), and that PMP22 overexpression in mice causes dysmyelination (Robaglia-Schlupp *et al.*, 2002).

Is membrane potential altered in CMT1A?

One of the aims of this study was to test for changes in axonal membrane properties which might be related to secondary axonal degeneration, such as membrane depolarization. Our recordings provide no evidence that membrane potential is appreciably abnormal in CMT1A. It might be argued that the raised thresholds and fanning out of TE are characteristics of membrane hyperpolarization. However, the early fanning out in CMT1A patients is very different from the fanning out seen in hyperpolarization, whether caused by DC currents, release of ischaemia, hypokalaemia or occurring in multifocal motor neuropathy (Kiernan and Bostock, 2000; Kiernan *et al.*, 2002*b*; Kuwabara *et al.*, 2002*b*), in which the deviation from normal increases during 100 ms hyperpolarization. In all of these examples of membrane hyperpolarization, superexcitability was increased relative to normal and relative to the late subexcitability. In CMT1A, however, the recovery cycle is relatively normal (Fig. 3), although refractoriness and superexcitability are significantly reduced. These changes in the recovery cycle are difficult to interpret in the presence of the substantial changes in passive membrane properties, but

are no more consistent with depolarization (which invariably increases refractoriness) than with hyperpolarization.

Comparison with other chronic demyelinating neuropathies

The results of the axonal excitability measures in the present study are different from those previously described in acquired demyelinating neuropathies, namely CIDP, multifocal motor neuropathy and Guillain–Barré syndrome, as described in the Introduction. Interestingly, a more recent study has found that a subset of CIDP patients, corresponding to those with a diffuse pattern of demyelination, exhibit features rather similar to those in CMT1A, namely increased thresholds, early fanning-out of TE, with increased activity of inward rectification on hyperpolarization (Sung *et al.*, 2004). There may be a contribution from endoneurial inflammation to the findings in these demyelinating neuropathies (Redford *et al.*, 1997), but it is unlikely that this plays a major role in CMT1A. It remains to be determined whether there are any consistent differences between the abnormal excitability properties in CMT1A and CIDP that could relate to the different aetiologies of demyelination.

Decreased nerve conduction velocity in CMT1A

Many factors may contribute to the decreased nerve conduction velocities typically seen in CMT1A, including axon diameter, myelin thickness and internodal distance. Recently, a few molecules, such as contactin, have been shown to play an important role in segregating nodes and juxtaparanodes and in anchoring Schwann cells to paranodes (Boyle *et al.*, 2001). The disruption of the paranodal junction alone in contactin mutant mice may account for the impaired conduction velocity (Boyle *et al.*, 2001). The disruption of the paranode is expected to reduce R_{il} (Fig. 6A), with consequent effects on excitability parameters, as found in CMT1A, as well as on conduction velocities (Boyle *et al.*, 2001; Kaji, 2003). An alternative explanation for the reduction in velocity is decreased Na^+ channel function (e.g. decreased density) (Kazarinova-Noyes *et al.*, 2001). However, our results did not support abnormal Na^+ channel function, as strength–duration time constant, a sensitive measure of persistent Na^+ current at the node, showed no significant change.

In summary, our data indicate that CMT1A patients exhibit a consistent pattern of abnormal nerve excitability properties. This pattern indicates increased access of applied currents to the internodal compartment of the axon and increased activation of fast K^+ channels. This is the first time that abnormal excitability properties have been found in a neuropathy that are logically attributable to altered myelination, and which may therefore aid the interpretation of excitability abnormalities in other conditions. However, the resemblance of the TE recordings to those in immature rats raises the possibility that the changes are related more specifically to nodal dysmaturity, and may differ in some respects from those in other demyelinating neuropathies.

References

Barrett EF, Barrett JN. Intracellular recording from vertebrate myelinated axons: mechanism of the depolarizing afterpotential. J Physiol 1982; 323: 117–44.

Birouk N, Gouider R, Le Guern E, Gugenheim M, Tardieu S, Maisonobe T, et al. Charcot–Marie–Tooth disease type 1A with 17p11.2 duplication. Clinical and electrophysiological phenotype study and factors influencing disease severity in 119 cases. Brain 1997; 120: 813–23.

Bostock H. Mechanisms of accommodation and adaptation in myelinated axons. In: Waxman SG, Kocsis JD, Stys PK, editors. The axon. New York: Oxford University Press; 1995. p. 311–27.

Bostock H, Sears TA, Sherratt RM. The effects of 4-aminopyridine and tetraethylammonium ions on normal and demyelinated mammalian nerve fibres. J Physiol 1981; 313: 301–15.

Bostock H, Cikurel K, Burke D. Threshold tracking technique in the study of human peripheral nerve. Muscle Nerve 1998; 21: 137–58.

Boyle ME, Berglund EO, Murai KK, Weber L, Peles E, Ranscht B. Contactin orchestrates assembly of the septate-like junctions at the paranode in myelinated peripheral nerve. Neuron 2001; 30: 385–97.

Brismar T. Specific permeability properties of demyelinated rat nerve fibres. Acta Physiol Scand 1981; 113: 167–76.

Burke D, Kiernan MC, Bostock H. Excitability of human axons. Clin Neurophysiol 2001; 112: 1575–85.

Cappelen-Smith C, Kuwabara S, Lin CS, Mogyoros I, Burke D. Membrane properties in chronic inflammatory demyelinating polyneuropathy. Brain 2001; 124: 2439–47.

Cappelen-Smith C, Kuwabara S, Lin CS, Burke D. Abnormalities of axonal excitability are not generalized in early multifocal motor neuropathy. Muscle Nerve 2002; 26: 769–76.

Chiu SY, Ritchie JM. Evidence for the presence of potassium channels in the paranodal region of acutely demyelinated mammalian single nerve fibres. J Physiol 1981; 313: 415–37.

Dyck PJ, Chance P, Lebo R, Carney AJ. Hereditary motor and sensory neuropathies. In: Dyck PJ, Thomas PK, Griffin JW, Low PA, Poduslo JF, editors. Peripheral neuropathy, 3rd edn. Philadelphia: W.B. Saunders; 1993. p. 1094–136.

Girault JA, Peles E. Development of nodes of Ranvier. Curr Opin Neurobiol 2002; 12: 476–85.

Hanemann CO, Gabreels-Festen AA. Secondary axon atrophy and neurological dysfunction in demyelinating neuropathies. Curr Opin Neurol 2002; 15: 611–5.

Hattori N, Yamamoto M, Yoshihara T, Koike H, Nakagawa M, Yoshikawa H, et al. Demyelinating and axonal features of Charcot–Marie–Tooth disease with mutations of myelin-related proteins (PMP22, MPZ and Cx32): a clinicopathological study of 205 Japanese patients. Brain 2003; 126: 134–51.

Kaji R. Physiological and technical basis of peripheral nerve and motoneurons testing. In: Kimura J, Kaji R, editors. Physiology of ALS and related diseases. Amsterdam: Elsevier; 1997. p. 15–41.

Kaji R. Physiology of conduction block in multifocal motor neuropathy and other demyelinating neuropathies. Muscle Nerve 2003; 27: 285–96.

Kaji R, Oka N, Tsuji T, Mezaki T, Nishio T, Akiguchi I, et al. Pathological findings at the site of conduction block in multifocal motor neuropathy. Ann Neurol 1993; 33: 152–8.

Kamholz J, Menichella D, Jani A, Garbern J, Lewis RA, Krajewski KM, et al. Charcot–Marie–Tooth disease type I. Molecular pathogenesis to gene therapy. Brain 2000; 123: 222–33.

Kazarinova-Noyes K, Malhotra JD, McEwen DP, Mattei LN, Berglund EO, Ransch B, et al. Contactin associates with Na+ channels and increases their functional expression. J Neurosci 2001; 21: 7517–25.

Kiernan MC, Bostock H. Effects of membrane polarization and ischaemia on